

1 Erosion of somatic tissue identity with loss of the X-linked  
2 intellectual disability factor KDM5C

3

4 Katherine M. Bonefas<sup>1,2</sup>, Ilakkia Venkatachalam<sup>2,3</sup>, and Shigeki Iwase<sup>2</sup>.

5 1. Neuroscience Graduate Program, University of Michigan Medical School, Ann Arbor, MI, 48109, USA.

6      2. Department of Human Genetics, Michigan Medicine, University of Michigan Medical School, Ann Arbor,  
7           MI, 48109, USA.

8 3. Genetics and Genomics Graduate Program, University of Michigan, Ann Arbor, MI, 48109, USA.

## 9 Abstract

10 Mutations in numerous chromatin-modifying enzymes cause neurodevelopmental disorders (NDDs) with  
11 unknown mechanisms. Loss of repressive chromatin regulators can lead to the aberrant transcription of  
12 tissue-specific genes outside of their intended context, however the mechanisms and consequences of their  
13 dysregulation are largely unknown. Here, we examine how lysine demethylase 5c (KDM5C), an eraser of  
14 histone 3 lysine 4 di and tri-methylation (H3K4me2/3) that is mutated in Claes-Jensen X-linked intellectual  
15 disability, contributes to tissue identity. We found male *Kdm5c* knockout (-KO) mice, which recapitulate  
16 key human neurological phenotypes, aberrantly expresses many liver, muscle, ovary, and testis genes  
17 within the amygdala and hippocampus. Gonad-enriched genes misexpressed in the *Kdm5c*-KO brain are  
18 unique to germ cells, indicating an erosion of the soma-germline boundary. Germline genes are typically  
19 decommissioned in somatic lineages in the post-implantation epiblast, yet *Kdm5c*-KO epiblast-like cells  
20 (EpiLCs) aberrantly expressed key regulators of germline identity and meiosis, including *Dazl* and *Stra8*.  
21 Germline gene repression is sexually dimorphic, as female EpiLCs required a higher dose of KDM5C to  
22 maintain germline gene suppression. Using a comprehensive list of mouse germline-enriched genes, we  
23 found KDM5C is selectively recruited to a subset of germline gene promoters that contain CpG islands  
24 (CGIs) to facilitate DNA CpG methylation (CpGme) during ESC to EpiLC differentiation. However, late stage  
25 spermatogenesis genes devoid of promoter CGIs can also become activated in *Kdm5c*-KO cells via ectopic  
26 activation by RFX transcription factors. Together, these data demonstrate KDM5C's fundamental role in  
27 tissue identity and indicate that KDM5C acts as a break against runaway activation of germline developmental  
28 programs in somatic lineages.

## 29 Introduction

30 A single genome holds the instructions to generate the myriad of cell types found within an organism.  
31 This is, in part, accomplished by chromatin regulators that can either promote or impede lineage-specific  
32 gene expression through DNA and histone modifications<sup>1–5</sup>. Human genetic studies revealed mutations in  
33 chromatin regulators are a major cause of neurodevelopmental disorders (NDDs)<sup>6</sup> and many studies have  
34 identified their importance for regulating brain-specific transcriptional programs. Loss of chromatin regulators  
35 can also result in the ectopic expression of tissue-specific genes outside of their target environment, such  
36 as the misexpression of liver-specific genes within adult neurons<sup>7</sup>. However, the mechanisms underlying  
37 ectopic gene expression and its impact upon neurodevelopment are poorly understood.

38 To elucidate the role of tissue identity in chromatin-linked NDDs, it is essential to first characterize the  
39 nature of the dysregulated genes and the molecular mechanisms governing their de-repression. Here we  
40 focus on lysine demethylase 5C (KDM5C, also known as SMCX or JARID1C), which erases histone 3 lysine  
41 4 di- and trimethylation (H3K4me2/3), a permissive chromatin modification enriched at gene promoters<sup>8</sup>.  
42 Pathogenic mutations in *KDM5C* cause Intellectual Developmental Disorder, X-linked, Syndromic, Claes-  
43 Jensen Type (MRXSCJ, OMIM: 300534). MRXSCJ is more common and severe in males and its neurological  
44 phenotypes include intellectual disability, seizures, aberrant aggression, and autistic behaviors<sup>9–11</sup>. Male  
45 *Kdm5c* knockout (-KO) mice recapitulate key MRXSCJ phenotypes, including hyperaggression, increased  
46 seizure propensity, social deficits, and learning impairments<sup>12–14</sup>. RNA sequencing (RNA-seq) of the  
47 *Kdm5c*-KO hippocampus revealed ectopic expression of some germline genes within the brain<sup>13</sup>. However,  
48 it is unclear if other tissue-specific genes are aberrantly transcribed with KDM5C loss, at what point in  
49 development germline gene misexpression begins, and what mechanisms underlie their dysregulation.

50 Distinguishing between germ cells and somatic cells is a key feature of multicellularity<sup>15</sup> that occurs  
51 during early embryogenesis in many metazoans<sup>16</sup>. In mammals, chromatin regulators are crucial for  
52 decommissioning germline genes during the transition from naïve to primed pluripotency. Initially, germline  
53 gene promoters gain repressive histone H2A lysine 119 monoubiquitination (H2AK119ub1)<sup>17</sup> and histone 3  
54 lysine 9 trimethylation (H3K9me3)<sup>17,18</sup> in embryonic stem cells (ESCs) and are then decorated with DNA  
55 CpG methylation (CpGme) in the post-implantation embryo<sup>18–21</sup>. The contribution of KDM5C to this process  
56 remains unclear. Additionally, studies on germline gene repression have primarily been conducted in males  
57 and focused on select marker genes important for germ cell development, given the lack of a comprehensive  
58 list for germline-enriched genes. Therefore, it is unknown if the mechanism of repression differs between  
59 sexes or for certain classes of germline genes, e.g. meiotic versus spermatid differentiation genes.

60 To illuminate KDM5C's role in tissue identity, here we characterized the aberrant expression of tissue-  
61 enriched genes within the *Kdm5c*-KO brain and epiblast-like stem cells (EpiLCs), an *in vitro* model of the  
62 post-implantation embryo. We curated a list of mouse germline-enriched genes, which enabled genome-wide  
63 analysis of germline gene silencing mechanisms for the first time. Based on the data presented below, we

64 propose KDM5C plays a fundamental, sexually dimorphic role in the development of tissue identity during  
65 early embryogenesis, including the establishment of the soma-germline boundary.

## 66 Results

### 67 **Tissue-enriched genes are aberrantly expressed in the *Kdm5c*-KO brain**

68 Previous RNA sequencing (RNA-seq) of the adult male *Kdm5c*-KO hippocampus revealed ectopic  
69 expression of some germline genes unique to the testis<sup>13</sup>. It is currently unknown if the testis is the only  
70 tissue type misexpressed in the *Kdm5c*-KO brain. We thus systematically tested whether other tissue-specific  
71 genes are misexpressed in the male brain with constitutive knockout of *Kdm5c* (*Kdm5c*<sup>-y</sup>, 5CKO)<sup>22</sup> by using  
72 a published list of mouse tissue-enriched genes<sup>23</sup>.

73 We found a large proportion of significantly upregulated genes (DESeq2<sup>24</sup>, log2 fold change > 0.5, q < 0.1)  
74 within the male *Kdm5c*-KO amygdala and hippocampus are non-brain, tissue-specific genes (Amygdala: 35%,  
75 Hippocampus: 24%) (Figure 1A-B). For both the amygdala and hippocampus, the majority of tissue-enriched  
76 differentially expressed genes (DEGs) were testis genes (Figure 1A-B). Even though the testis has the  
77 largest total number of tissue-biased genes (2,496 genes) compared to any other tissue, testis-biased DEGs  
78 were significantly enriched for both brain regions (Amygdala p = 1.83e-05, Odds Ratio = 5.13; Hippocampus  
79 p = 4.26e-11, Odds Ratio = 4.45, Fisher's Exact Test). An example of a testis-enriched gene misexpressed  
80 in the *Kdm5c*-KO brain is *FK506 binding protein 6* (*Fkbp6*), a known regulator of PIWI-interacting RNAs  
81 (piRNAs) and meiosis<sup>25,26</sup> (Figure 1C).

82 Interestingly, we also observed significant enrichment of ovary-biased genes in both the amygdala and  
83 hippocampus (Amygdala p = 0.00574, Odds Ratio = 18.7; Hippocampus p = 0.048, Odds Ratio = 5.88,  
84 Fisher's Exact) (Figure 1A-B). Ovary-enriched DEGs included *Zygotic arrest 1* (*Zar1*), which sequesters  
85 mRNAs in oocytes for meiotic maturation<sup>27</sup> (Figure 1D). Given that the *Kdm5c*-KO mice we analyzed are  
86 male, these data demonstrate that the ectopic expression of gonad-enriched genes is independent of  
87 organismal sex.

88 Although not consistent across brain regions, we also found significant enrichment of genes biased  
89 towards two non-gonadal tissues - the liver (Amygdala p = 0.04, Odds Ratio = 6.58, Fisher's Exact Test) and  
90 muscles (Hippocampus p = 0.01, Odds Ratio = 6.95, Fisher's Exact Test) (Figure 1A-B). *Apolipoprotein C-I*  
91 (*Apoc1*) a lipoprotein metabolism and transport gene, is among the liver-biased DEG derepressed in both  
92 the hippocampus and amygdala<sup>28</sup> and its brain overexpression has been implicated in Alzheimer's disease<sup>29</sup>  
93 (Figure 1E).

94 Analysis of oligo(dT)-primed libraries<sup>22</sup> demonstrates aberrantly expressed mRNAs are polyadenylated  
95 and spliced into mature transcripts in the *Kdm5c*-KO brain (Figure 1C-E). Of note, we observed little to no  
96 dysregulation of brain-enriched genes (Amygdala p = 1, Odds Ratio = 1.22; Hippocampus p = 0.74, Odds

97 Ratio = 1.22, Fisher's Exact), despite the fact these are brain samples and the brain has the second highest  
98 total number of tissue-enriched genes (708 genes). Altogether, these results suggest the aberrant expression  
99 of tissue-enriched genes within the brain is a major effect of KDM5C loss.

100 **Germline genes are misexpressed in the *Kdm5c*-KO brain**

101 *Kdm5c*-KO brain expresses testicular germline genes<sup>13</sup>, however the testis also contains somatic cells that  
102 support hormone production and germline functions. To determine if *Kdm5c*-KO results in ectopic expression  
103 of somatic testicular genes, we first evaluated the known functions of testicular DEGs through gene ontology.  
104 We found *Kdm5c*-KO testis-enriched DEGs had high enrichment of germline-relevant ontologies, including  
105 spermatid development (GO: 0007286, p.adjust = 6.2e-12) and sperm axoneme assembly (GO: 0007288,  
106 p.adjust = 2.45e-14) (Figure 2A).

107 We then evaluated testicular DEG expression in wild-type testes versus testes with germ cell depletion<sup>30</sup>,  
108 which was accomplished by heterozygous *W* and *Wv* mutations in the enzymatic domain of *c-Kit* (*Kit*<sup>W/Wv</sup>)<sup>31</sup>.  
109 Almost all *Kdm5c*-KO testis-enriched DEGs lost expression with germ cell depletion (Figure 2B). We then  
110 assessed testis-enriched DEG expression in a published single cell RNA-seq dataset that identified cell  
111 type-specific markers within the testis<sup>32</sup>. Some *Kdm5c*-KO testis-enriched DEGs were classified as specific  
112 markers for different germ cell developmental stages (e.g. spermatogonia, spermatocytes, round spermatids,  
113 and elongating spermatids), yet none marked somatic cells (Figure 2C). Together, these data demonstrate  
114 that the *Kdm5c*-KO brain aberrantly expresses germline genes but not somatic testicular genes, reflecting an  
115 erosion of the soma-germline boundary.

116 As of yet, research on germline gene silencing mechanisms has focused on a handful of key genes rather  
117 than assessing germline gene suppression genome-wide, due to the lack of a comprehensive gene list.  
118 We therefore generated a list of mouse germline-enriched genes using RNA-seq datasets of *Kit*<sup>W/Wv</sup> mice  
119 that included males and females at embryonic day 12, 14, and 16<sup>33</sup> and adult male testes<sup>30</sup>. We defined  
120 genes as germline-enriched if their expression met the following criteria: 1) their expression is greater than  
121 1 FPKM in wild-type gonads 2) their expression in any non-gonadal tissue of adult wild type mice<sup>23</sup> does  
122 not exceed 20% of their maximum expression in the wild-type germline, and 3) their expression in the germ  
123 cell-depleted gonads, for any sex or time point, does not exceed 20% of their maximum expression in the  
124 wild-type germline. These criteria yielded 1,288 germline-enriched genes (Figure 2D), which was hereafter  
125 used as a resource to globally characterize germline gene misexpression with *Kdm5c* loss (Supplementary  
126 table 1).

127 ***Kdm5c*-KO epiblast-like cells aberrantly express key regulators of germline identity**

128 Germ cells are typically distinguished from somatic cells soon after the embryo implants into the uterine  
129 wall<sup>34,35</sup>, when germline genes are silenced in epiblast stem cells that will form the somatic tissues<sup>36</sup>. This

130 developmental time point can be modeled *in vitro* through differentiation of naïve embryonic stem cells  
131 (nESCs) into epiblast-like stem cells (EpiLCs) (Figure 3A)<sup>37,38</sup>. While some germline-enriched genes are  
132 also expressed in nESCs and in the 2-cell stage<sup>39–41</sup>, they are silenced as they differentiate into EpiLCs<sup>18,19</sup>.  
133 Therefore, we tested if KDM5C was necessary for the initial silencing of germline genes in somatic lineages  
134 by evaluating the impact of *Kdm5c* loss in male EpiLCs.

135 *Kdm5c*-KO cell morphology during ESC to EpiLC differentiation appeared normal (Figure 3B) and EpiLCs  
136 properly expressed markers of primed pluripotency, such as *Dnmt3b*, *Fgf5*, *Pou3f1*, and *Otx2* (Figure 3C). We  
137 then identified tissue-enriched DEGs in a RNA-seq dataset of wild-type and *Kdm5c*-KO EpiLCs<sup>42</sup> (DESeq2,  
138 log<sub>2</sub> fold change > 0.5, q < 0.1). Similar to the *Kdm5c*-KO brain, we observed general dysregulation of  
139 tissue-enriched genes, with the largest number of genes belonging to the brain and testis, although they  
140 were not significantly enriched (Figure 3D). Using our list of mouse germline-enriched genes assembled  
141 above, we identified 68 germline genes misexpressed in male *Kdm5c*-KO EpiLCs.

142 We then compared EpiLC germline DEGs to those expressed in the *Kdm5c*-KO brain to determine if  
143 germline genes are constitutively dysregulated or change over the course of development. The majority of  
144 germline DEGs were unique to either EpiLCs or the brain, with only *D1Pas1* and *Cyct* shared across all  
145 tissue/cell types (Figure 3E-F). EpiLC germline DEGs had particularly high enrichment of meiosis-related  
146 gene ontologies when compared to the brain (Figure 3G), such as meiotic cell cycle process (GO:1903046,  
147 p.adjust = 2.2e-07) and meiotic nuclear division (GO:0140013, p.adjust = 1.37e-07). While there was  
148 modest enrichment of meiotic gene ontologies in both brain regions, the *Kdm5c*-KO hippocampus primarily  
149 expressed late-stage spermatogenesis genes involved in sperm axoneme assembly (GO:0007288, p.adjust  
150 = 0.00621) and sperm motility (GO:0097722, p.adjust = 0.00612).

151 Notably, DEGs unique to *Kdm5c*-KO EpiLCs included key drivers of germline identity, such as *Stimulated*  
152 *by retinoic acid 8* (*Stra8*: log<sub>2</sub> fold change = 3.73, q = 2.17e-39) and *Deleted in azoospermia like* (*Dazl*: log<sub>2</sub>  
153 fold change = 3.36, q = 3.19e-12) (Figure 3H). These genes are typically expressed when primordial germ  
154 cells (PGCs) are committed to the germline fate and again later in life to trigger meiotic gene expression  
155 programs<sup>43–45</sup>. Of note, some germline genes, including *Dazl*, are also expressed in the two-cell embryo<sup>40,46</sup>.  
156 However, we did not see derepression of two-cell stage-specific genes, like *Duxf3* (*Dux*) (log<sub>2</sub> fold change  
157 = -0.282, q = 0.337) and *Zscan4d* (log<sub>2</sub> fold change = 0.25, q = 0.381) (Figure 3H), indicating *Kdm5c*-KO  
158 EpiLCs do not revert back to a 2-cell state. Altogether, *Kdm5c*-KO EpiLCs express key drivers of germline  
159 identity and meiosis while the brain primarily expresses spermiogenesis genes, indicating germline gene  
160 misexpression mirrors germline development during the progression of somatic development.

161 **Female epiblast-like cells have increased sensitivity to germline gene misexpression**  
162 **with *Kdm5c* loss**

163 It is currently unknown if the misexpression of germline genes is influenced by sex, as previous studies  
164 on germline gene repressors have focused on male cells<sup>17,18,20,47,48</sup>. Sex is particularly pertinent in the case  
165 of KDM5C because it partially escapes X chromosome inactivation (XCI), resulting in a higher dosage in  
166 females<sup>49–52</sup>. We therefore explored the impact of chromosomal sex upon germline gene suppression by  
167 comparing their dysregulation in male *Kdm5c* hemizygous knockout (XY *Kdm5c*-KO, XY 5CKO), female  
168 homozygous knockout (XX *Kdm5c*-KO, XX 5CKO), and female heterozygous knockout (XX *Kdm5c*-HET, XX  
169 5CHET) EpiLCs<sup>42</sup>.

170 In EpiLCs, homozygous and heterozygous *Kdm5c* knockout females expressed over double the number  
171 of germline-enriched genes than hemizygous males (Figure 4A). While the majority of germline DEGs in  
172 *Kdm5c*-KO males were also dysregulated in females (74%), many were sex-specific, such as *Tktl2* and *Esx1*  
173 (Figure 4B). We then compared the known functions of germline genes dysregulated only in females, only in  
174 males, or in all samples (Figure 4C). Female-specific germline DEGs were enriched for meiotic (GO:0051321  
175 - meiotic cell cycle) and flagellar (GO:0003341 - cilium movement) functions, while male-specific DEGs had  
176 roles in mitochondrial and cell signaling (GO:0070585 - protein localization to mitochondrion). Germline  
177 transcripts expressed in both sexes were enriched for meiotic (GO:0140013 - meiotic nuclear division) and  
178 egg-specific functions (GO:0007292 - female gamete generation).

179 The majority of germline genes expressed in both sexes were more highly dysregulated in females  
180 compared to males (Figure 4D-F). This increased degree of dysregulation in females, along with the  
181 increased total number of germline genes, indicates females are more sensitive to losing KDM5C-mediated  
182 germline gene suppression. Heightened germline gene dysregulation in females could be due to impaired  
183 XCI in *Kdm5c* mutants<sup>42</sup>, as many spermatogenesis genes lie on the X chromosome<sup>53,54</sup>. However, female  
184 germline DEGs were not biased towards the X chromosome and females had a similar overall proportion  
185 of germline DEGs belonging to the X chromosome as males (XY *Kdm5c*-KO - 10.29%, XX *Kdm5c*-HET -  
186 7.43%, XX *Kdm5c*-KO - 10.59%) (Figure 4G). The majority of germline DEGs instead lie on autosomes for  
187 both male and female *Kdm5c* mutants (Figure 4G). Thus, while female EpiLCs are more prone to germline  
188 gene misexpression with KDM5C loss, it is likely independent of XCI defects.

189 **Germline gene misexpression in *Kdm5c* mutants is independent of germ cell sex**

190 Although many germline genes have shared functions in the male and female germline, e.g. PGC  
191 formation, meiosis, and genome defense, some have unique or sex-biased expression. Therefore, we  
192 wondered if *Kdm5c* mutant males would primarily express sperm genes while mutant females would primarily  
193 express egg genes. To comprehensively assess whether germline gene sex corresponds with *Kdm5c* mutant  
194 sex, we first filtered our list of germline-enriched genes for egg and sperm-biased genes (Figure 4H). We

195 defined germ cell sex-biased genes as those whose expression in the opposite sex, at any time point, is  
196 no greater than 20% of the gene's maximum expression in a given sex. This criteria yielded 0 egg-biased,  
197 0 sperm-biased, and 197 unbiased germline-enriched genes. We found regardless of sex, egg, sperm,  
198 and unbiased germline genes were dysregulated in all *Kdm5c* mutants at similar proportions (Figure 4I-J).  
199 Furthermore, germline genes dysregulated exclusively in either male or female mutants were also not biased  
200 towards their corresponding germ cell sex (Figure 4I). Altogether, these results demonstrate sex differences  
201 in germline gene dysregulation is not due to sex-specific activation of sperm or egg transcriptional programs.

## 202 **KDM5C binds to a subset of germline gene promoters during early embryogenesis**

203 KDM5C binds to the promoters of several germline genes in embryonic stem cells (ESCs) but not in  
204 neurons<sup>13,55</sup>. However, the lack of a comprehensive list of germline-enriched genes prohibited genome-wide  
205 characterization of KDM5C binding at germline gene promoters. Thus, it is unclear if KDM5C is enriched at  
206 germline gene promoters, what types of germline genes KDM5C regulates, and if its binding is maintained at  
207 any germline genes in neurons.

208 To address these questions, we analyzed KDM5C chromatin immunoprecipitation followed by DNA  
209 sequencing (ChIP-seq) datasets in EpiLCs<sup>42</sup> and primary forebrain neuron cultures (PNCs)<sup>12</sup> (MACS2 q  
210 < 0.1, fold enrichment > 1, and removal of false-positive peaks in *Kdm5c*-KO). EpiLCs had a higher total  
211 number of high-confidence KDM5C peaks than PNCs (EpiLCs: 5,808, PNCs: 1,276). KDM5C was primarily  
212 localized to gene promoters in both cell types (promoters = transcription start site (TSS) ± 500 bp, EpiLCs:  
213 4,190, PNCs: 745), although PNCs showed increased localization to non-promoter regions (Figure 5A).

214 The majority of promoters bound by KDM5C in PNCs were also bound in EpiLCs (513 shared promoters),  
215 however a large portion of gene promoters were bound by KDM5C only in EpiLCs (3,677 EpiLC only  
216 promoters) (Figure 5B). Genes bound by KDM5C in both PNCs and EpiLCs were enriched for functions  
217 involving nucleic acid turnover, such as deoxyribonucleotide metabolic process (GO:0009262, p.adjust =  
218 8.28e-05) (Figure 5C). Germline ontologies were enriched only in EpiLC-specific, KDM5C-bound promoters,  
219 such as meiotic nuclear division (GO: 0007127 p.adjust = 6.77e-16) (Figure 5C). There were no significant  
220 ontologies for PNC-specific KDM5C target genes. Using our mouse germline gene list, we observed evident  
221 KDM5C signal around the TSS of many germline genes in EpiLCs, but not in PNCs (Figure 5D). Based  
222 on our ChIP-seq peak cut-off criteria, KDM5C was highly enriched at 211 germline gene promoters in  
223 EpiLCs (16.4% of all germline genes) (Figure 5E). Of note, KDM5C was only bound to about one third  
224 of RNA-seq DEG promoters unique to EpiLCs or the brain (EpiLC only DEGs: 34.9%, Brain only DEGs:  
225 30%) (Supplementary figure 1A-C). Representative examples of EpiLC DEGs bound and unbound by  
226 KDM5C in EpiLCs are *Dazl* and *Stra8*, respectively (Figure 5F). However, the four of the five germline genes  
227 dysregulated in both EpiLCs and the brain were bound by KDM5C in EpiLCs (*D1Pas1*, *Hsf2bp*, *Cyct*, and  
228 *Stk31*) (Supplementary figure 1A). Together, these results demonstrate KDM5C is recruited to a subset  
229 of germline genes in EpiLCs, including meiotic genes, but does not directly regulate germline genes in

230 neurons. Furthermore, the majority of germline mRNAs expressed in *Kdm5c*-KO cells are dysregulated  
231 independent of direct KDM5C recruitment to their gene promoters, however genes dysregulated across  
232 *Kdm5c*-KO development are often direct KDM5C targets.

233 Many germline-specific genes are suppressed by the polycomb repressive complex 1.6 (PRC1.6), which  
234 contains transcription factor heterodimers E2F6/DP1 and MGA/MAX that respectively bind E2F and E-box  
235 motifs<sup>58</sup>. PRC1.6 members may recruit KDM5C to germline gene promoters<sup>13</sup>, given their association  
236 with KDM5C in HeLa cells and ESCs<sup>46,59</sup>. We thus used HOMER<sup>60</sup> to identify transcription factor motifs  
237 enriched at KDM5C-bound or unbound germline gene promoters (TSS ± 500 bp, q-value < 0.1). MAX  
238 and E2F6 binding sites were significantly enriched at germline genes bound by KDM5C in EpiLCs (MAX  
239 q-value: 0.0068, E2F6 q-value: 0.0673, E2F q-value: 0.0917), but not at germline genes unbound by  
240 KDM5C (Figure 5G). One third of KDM5C-bound promoters contained the consensus sequence for either  
241 E2F6 (E2F, 5'-TCCCGC-3'), MGA (E-box, 5'-CACGTG-3'), or both, but only 17% of KDM5C-unbound genes  
242 contained these motifs (Figure 5H). KDM5C-unbound germline genes were instead enriched for multiple  
243 RFX transcription factor binding sites (RFX q-value < 0.0001, RFX2 q-value < 0.0001, RFX5 q-value <  
244 0.0001) (Figure 5I, Supplementary figure 1D). RFX transcription factors bind X-box motifs<sup>61</sup> to promote  
245 ciliogenesis<sup>62,63</sup> and among them is RFX2, a central regulator of post-meiotic spermatogenesis<sup>64,65</sup>. Although  
246 *Rfx2* is also not a direct target of KDM5C (Supplementary figure 1E), RFX2 mRNA is derepressed in *Kdm5c*-  
247 KO EpiLCs (Figure 5J). Thus, RFX2 is a candidate transcription factor for driving the ectopic expression of  
248 many KDM5C-unbound germline genes in *Kdm5c*-KO cells.

249 **KDM5C is recruited to CpG islands at germline promoters to facilitate *de novo* DNA  
250 methylation**

251 Previous work found two germline gene promoters have a marked reduction in DNA CpG methylation  
252 (CpGme) in the *Kdm5c*-KO adult hippocampus<sup>13</sup>. Since histone 3 lysine 4 di- and trimethylation (H3K4me2/3)  
253 impede *de novo* CpGme<sup>66,67</sup>, KDM5C's removal of H3K4me2/3 may be required to suppress germline  
254 genes. However, KDM5C's catalytic activity was recently shown to be dispensable for suppressing *Dazl* in  
255 undifferentiated ESCs<sup>46</sup>. To reconcile these observations, we hypothesized KDM5C erases H3K4me2/3 to  
256 promote the initial placement of CpGme at germline gene promoters in EpiLCs.

257 To test this hypothesis, we first characterized KDM5C's expression as naïve ESCs differentiate into  
258 EpiLCs (Figure 6A). While *Kdm5c* mRNA steadily decreased from 0 to 48 hours of differentiation (Figure  
259 6B), KDM5C protein initially increased from 0 to 24 hours but then decreased to near knockout levels by 48  
260 hours (Figure 6C). We then characterized KDM5C's substrates (H3K4me2/3) at germline gene promoters  
261 with *Kdm5c* loss using published ChIP-seq datasets<sup>22,42</sup>. *Kdm5c*-KO samples showed a marked increase in  
262 H3K4me2 in EpiLCs (Figure 6D) and H3K4me3 in the amygdala (Figure 6E) around the TSS of germline  
263 genes. Together, these data suggest KDM5C acts during the transition between ESCs and EpiLCs to remove

264 H3K4me2/3 at germline gene promoters.  
265 Germline genes accumulate CpG methylation (CpGme) at CpG islands (CGIs) during the transition  
266 from naïve to primed pluripotency<sup>19,21,68</sup>. We first examined how many of our germline-enriched genes had  
267 promoter CGIs (TSS ± 500 bp) using the UCSC genome browser<sup>69</sup>. Notably, out of 1,288 germline-enriched  
268 genes, only 356 (27.64%) had promoter CGIs (Figure 6F). CGI-containing germline genes had higher  
269 enrichment of meiotic gene ontologies compared to CGI-free genes, including meiotic nuclear division  
270 (GO:0140013, p.adjust = 2.17e-12) and meiosis I (GO:0007127, p.adjust = 3.91e-10) (Figure 6G). Germline  
271 genes with promoter CGIs were more highly expressed than CGI-free genes across spermatogenesis  
272 stages, with highest expression in meiotic spermatocytes (Figure 6H). Contrastingly, CGI-free genes only  
273 displayed substantial expression in post-meiotic round spermatids (Figure 6H). Although only a minor portion  
274 of germline gene promoters contained CGIs, CGIs strongly determined KDM5C's recruitment to germline  
275 genes ( $p = 2.37e-67$ , Odds Ratio = 17.8, Fisher's exact test), with 79.15% of KDM5C-bound germline gene  
276 promoters harboring CGIs (Figure 6F).

277 To assess how KDM5C loss impacts initial CpGme placement at germline gene promoters, we performed  
278 whole genome bisulfite sequencing (WGBS) in male wild-type and *Kdm5c*-KO ESCs and 96-hour extend  
279 EpiLCs (exEpiLCs), when germline genes reach peak methylation levels<sup>18</sup> (Figure 6I). We first identified  
280 which germline gene promoters significantly gained CpGme in wild-type cells during nESC to exEpiLCs  
281 differentiation (methylKit<sup>70</sup>,  $q < 0.01$ ,  $|methylation\ difference| > 25\%$ , TSS ± 500 bp). In wild-type cells, the  
282 majority of germline genes gained substantial CpGme at their promoter during differentiation (60.08%),  
283 regardless if their promoter contained a CGI (Figure 6J).

284 We then identified promoters differentially methylated in wild-type versus *Kdm5c*-KO exEpiLCs (methylKit,  
285  $q < 0.01$ ,  $|methylation\ difference| > 25\%$ , TSS ± 500 bp). Of the 48,882 promoters assessed, 274 promoters  
286 were significantly hypomethylated and 377 promoters were significantly hypermethylated with KDM5C loss  
287 (Supplementary figure 2A). Many promoters hyper- and hypomethylated in *Kdm5c*-KO exEpiLCs belonged to  
288 genes with unknown functions. Hypomethylated promoters were significantly enriched for germline gene  
289 ontologies, such as meiotic nuclear division (GO:0140013, p.adjust = 0.012) (Supplementary figure 2B),  
290 with 10.22% of hypomethylated promoters belonging to germline genes. Approximately half of germline  
291 promoters hypomethylated in *Kdm5c*-KO exEpiLCs are direct targets of KDM5C in EpiLCs (13 out of 28  
292 hypomethylated promoters).

293 Promoters that showed the most robust loss of CpGme in *Kdm5c*-KO exEpiLCs (lowest q-values) harbored  
294 CGIs (Figure 6K). CGI promoters, but not CGI-free promoters, had a significant reduction in CpGme with  
295 KDM5C loss as a whole (Figure 6L) (Non-CGI promoters  $p = 0.0846$ , CGI promoters  $p = 0.0081$ , Mann-  
296 Whitney U test). Significantly hypomethylated promoters included germline genes consistently dysregulated  
297 across multiple *Kdm5c*-KO RNA-seq datasets<sup>13</sup>, such as *D1Pas1* (methylation difference = -60.03%, q-value  
298 = 3.26e-153) and *Naa11* (methylation difference = -42.45%, q-value = 1.44e-38) (Figure 6M). Surprisingly,  
299 we found only a modest reduction in CpGme at *Dazl*'s promoter (methylation difference = -6.525%, q-value =

300 0.0159) (Figure 6N). Altogether, these results demonstrate KDM5C is recruited to germline gene CGIs in  
301 EpiLCs to promote CpGme at germline gene promoters. Furthermore, this suggests while KDM5C's catalytic  
302 activity is required for the repression of some germline genes, CpGme can be placed at others even with  
303 elevated H3K4me2/3 around the TSS.

## 304 Discussion

305 In the above study, we demonstrate KDM5C's pivotal role in the development of tissue identity. We first  
306 characterized tissue-enriched genes expressed within the mouse *Kdm5c*-KO brain and identified substantial  
307 derepression of testis, liver, muscle, and ovary-enriched genes. Testis genes significantly enriched within the  
308 *Kdm5c*-KO amygdala and hippocampus are specific to the germline and absent in somatic cells. *Kdm5c*-KO  
309 epiblast-like cells (EpiLCs) aberrantly express key drivers of germline identity and meiosis, including *Dazl* and  
310 *Stra8*, while the adult brain primarily expresses genes important for late spermatogenesis. We demonstrated  
311 that although sex did not influence whether sperm or egg-specific genes were misexpressed, female EpiLCs  
312 have heightened germline gene de-repression with KDM5C loss. Germline genes can become aberrantly  
313 expressed in *Kdm5c*-KO cells via indirect mechanisms, such as activation through ectopic RFX transcription  
314 factors. Finally, we found KDM5C is dynamically regulated during ESC to EpiLC differentiation to promote  
315 long-term germline gene silencing through DNA methylation at CpG islands. Therefore, we propose KDM5C  
316 plays a fundamental role in the development of tissue identity during early embryogenesis, including the  
317 establishment of the soma-germline boundary. By systematically characterizing KDM5C's role in germline  
318 gene repression, we unveiled unique mechanisms governing the misexpression of distinct germline gene  
319 classes within somatic lineages. Ultimately, these data provide molecular footholds which can be exploited to  
320 test the overarching contribution of ectopic germline gene expression upon neurodevelopment.

321 By comparing *Kdm5c* mutant males and females, we revealed germline gene suppression is sexually  
322 dimorphic. While sex did not determine whether egg or sperm-specific genes were dysregulated, it greatly  
323 influenced the degree of germline gene dysregulation. Female EpiLCs are more severely impacted by loss  
324 of KDM5C-mediated germline gene suppression, yet this difference is not due to the increased number of  
325 germline genes on the X chromosome<sup>53,54</sup>. Increased germline gene misexpression in females may be  
326 related to females having a higher dose of KDM5C than males, due to its escape from XCI<sup>49–52</sup>. Intriguingly,  
327 heterozygous knockout females (*Kdm5c*<sup>+/−</sup>) also had over double the number of germline DEGs than  
328 hemizygous knockout males (*Kdm5c*<sup>−/Y</sup>), even though their expression of KDM5C should be roughly equivalent  
329 to that of wild-type males (*Kdm5c*<sup>+/Y</sup>). Males could partially compensate for KDM5C's loss via the Y-  
330 chromosome homolog, KDM5D. However, KDM5D exhibits weaker demethylase activity than KDM5C<sup>8</sup> and  
331 has not been reported to regulate germline gene expression. Altogether, these results demonstrate germline  
332 gene silencing mechanisms differ between males and females, which warrants further study to elucidate the  
333 biological ramifications and underlying mechanisms.

334 We found KDM5C is largely dispensable for promoting normal gene expression during development, yet  
335 is critical for suppressing ectopic developmental programs. It is important to note that while we highlighted  
336 KDM5C's repression of germline genes, some germline-enriched genes like *Dazl* are also expressed at the 2-  
337 cell stage and in naïve ESCs/the inner cell mass for their role in pluripotency and self-renewal<sup>41,46,71,72</sup>. These  
338 "self-renewal" germline genes are then silenced during ESC differentiation into epiblast stem cells/EpiLCs<sup>18,19</sup>.  
339 We found that while *Kdm5c*-KO EpiLCs express *Dazl*, they did not express 2-cell-specific genes like *Zscan4c*.  
340 These data suggest the 2-cell-like state reported in *Kdm5c*-KO ESCs<sup>46</sup> likely reflects KDM5C's primary  
341 role in germline gene repression. Germline gene misexpression in *Kdm5c*-KO EpiLCs may indicate they  
342 are differentiating into primordial germ cell-like cells (PGCLCs)<sup>34,35,37</sup>. Yet, *Kdm5c*-KO EpiLCs had normal  
343 cellular morphology and properly expressed markers for primed pluripotency, including *Otx2* which blocks  
344 EpiLC differentiation into PGCs/PGCLCs<sup>73</sup>. In addition to unimpaired EpiLC differentiation, *Kdm5c*-KO gross  
345 brain morphology is overall normal<sup>12</sup> and hardly any brain-specific genes were significantly dysregulated in  
346 the amygdala and hippocampus. Thus, ectopic germline gene expression occurs in conjunction with overall  
347 proper somatic differentiation in *Kdm5c*-KO animals.

348 Our work provides novel insight into the cross-talk between H3K4me2/3 and CpGme, which are gen-  
349 erally mutually exclusive<sup>74</sup>. In EpiLCs, loss of KDM5C binding at a subset of germline gene promoters,  
350 e.g. *D1Pas1*, strongly impaired promoter CGI methylation and resulted in their long-lasting de-repression into  
351 adulthood. Removal of H3K4me2/3 at CGIs is a plausible mechanism for KDM5C-mediated germline gene  
352 suppression<sup>13,55</sup>, given H3K4me2/3 can oppose DNMT3 activity<sup>66,67</sup>. However, emerging work indicates  
353 many histone-modifying enzymes have non-catalytic functions that influence gene expression, sometimes  
354 even more potently than their catalytic roles<sup>75,76</sup>. Indeed, KDM5C's catalytic activity was recently found to be  
355 dispensible for repressing *Dazl* in ESCs<sup>46</sup>. In our study, *Dazl*'s promoter still gained CpGme in *Kdm5c*-KO  
356 exEpiLCs, even with elevated H3K4me2. *Dazl* and a few other germline genes employ multiple repressive  
357 mechanisms to facilitate CpGme, such as DNMT3A/B recruitment via E2F6 and MGA<sup>17,18,47,48</sup>. This suggests  
358 alternative silencing mechanisms are sufficient to recruit DNMT3s to some germline CGIs, while others may  
359 require KDM5C-mediated H3K4me removal to overcome promoter CGI escape from CpGme<sup>74,77</sup>. These  
360 results also suggest the requirement for KDM5C's catalytic activity can change depending upon the locus  
361 and developmental stage, even for the same class of genes. However, further experiments are required to  
362 determine if catalytically inactive KDM5C can suppress germline genes at later developmental stages.

363 By generating a comprehensive list of mouse germline-enriched genes, we were able to reveal distinct  
364 derepressive mechanisms governing early versus late-stage germline developmental programs. Previous  
365 work on germline gene silencing has focused on genes with promoter CGIs<sup>19,74</sup>, and indeed the major-  
366 ity of KDM5C targets in EpiLCs were germ cell identity genes harboring CGIs. However, over 70% of  
367 germline-enriched gene promoters lacked CGIs, including the many KDM5C-unbound germline genes  
368 that are de-repressed in *Kdm5c*-KO cells. CGI-free, KDM5C-unbound germline genes were primarily  
369 late-stage spermatogenesis genes and significantly enriched for RFX2 binding sites, a central regulator

370 of spermiogenesis<sup>64,65</sup>. These data suggest that once activated during early embryogenesis, drivers of  
371 germline identity like *Rfx2*, *Stra8*, and *Dazl* turn on downstream germline programs, ultimately culminating in  
372 the expression of spermiogenesis genes in the adult *Kdm5c*-KO brain. Therefore, we propose KDM5C is  
373 recruited via promoter CGIs to act as a break against runaway activation of germline-specific programs.

374 The above work provides the mechanistic foundation for KDM5C-mediated repression of tissue and  
375 germline-specific genes. However, the contribution of these ectopic, tissue-specific genes towards *Kdm5c*-  
376 KO neurological impairments is still unknown. In addition to germline genes, we also identified significant  
377 enrichment of muscle and liver-biased transcripts within the *Kdm5c*-KO brain. Intriguingly, select liver and  
378 muscle-biased DEGs do have known roles within the brain, such as the liver-enriched lipid metabolism gene  
379 *Apolipoprotein C-I (Apoc1)*<sup>28</sup>. *APOC1* dysregulation is implicated in Alzheimer's disease in humans<sup>29</sup> and  
380 overexpression of *Apoc1* in the mouse brain can impair learning and memory<sup>78</sup>. KDM5C may therefore be  
381 crucial for neurodevelopment by fine-tuning the expression of tissue-enriched, dosage-sensitive genes like  
382 *Apoc1*.

383 Given that germline genes have no known functions within the brain, their impact upon neurodevelopment  
384 is currently unknown. In *C. elegans*, somatic misexpression of germline genes via loss of *Retinoblastoma*  
385 (*Rb*) homologs results in enhanced piRNA signaling and ectopic P granule formation in neurons<sup>79,80</sup>. Ectopic  
386 testicular germline transcripts have also been observed in a variety of cancers, including brain tumors in  
387 *Drosophila* and mammals<sup>81,82</sup> and shown to promote cancer progression<sup>83-85</sup>. Intriguingly, mouse models  
388 and human cells for other chromatin-linked NDDs also display impaired soma-germline demarcation<sup>86-88</sup>,  
389 such as mutations in DNA methyltransferase 3b (DNMT3B), H3K9me1/2 methyltransferases G9A/GLP,  
390 and methyl-CpG -binding protein 2 (MECP2). Recently, the transcription factor ZMYM2 (ZNF198), whose  
391 mutation causes neurodevelopmental-craniofacial syndrome with variable renal and cardiac abnormalities  
392 (OMIM #619522), was also shown to repress germline genes by promoting H3K4 methylation removal and  
393 CpGme<sup>89</sup>. Thus, KDM5C is among a growing cohort of neurodevelopmental disorders that have erosion of  
394 the germline-soma boundary. Further research is required to determine the impact of these germline genes  
395 upon neuronal functions and the extent to which this phenomenon occurs in humans.

## 396 Materials and Methods

### 397 Classifying tissue-enriched and germline-enriched genes

398 Tissue-enriched differentially expressd genes (DEGs) were determined by their classification in a previ-  
399 ously published dataset from 17 male and female mouse tissues<sup>23</sup>. This study defined tissue expression as  
400 greater than 1 Fragments Per Kilobase of transcript per Million mapped read (FPKM) and tissue enrichment  
401 as at least 4-fold higher expression than any other tissue.

402 We curated a list of germline-enriched genes using an RNA-seq dataset from wild-type and germline-

403 depleted (*Kit*<sup>W/W<sup>v</sup></sup>) male and female mouse embryos from embryonic day 12, 14, and 16<sup>33</sup>, as well as adult  
404 male testes<sup>30</sup>. Germline-enriched genes met the following criteria: 1) their expression is greater than 1  
405 FPKM in wild-type germline 2) their expression in any wild-type somatic tissues<sup>23</sup> does not exceed 20%  
406 of maximum expression in wild-type germline, and 3) their expression in the germ cell-depleted (*Kit*<sup>W/W<sup>v</sup></sup>)  
407 germline, for any sex or time point, does not exceed 20% of maximum expression in wild-type germline. We  
408 defined sperm and egg-biased genes as those whose expression in the opposite sex, at any time point, is no  
409 greater than 20% of the gene's maximum expression in a given sex. Genes that did not meet this threshold  
410 for either sex were classified as 'unbiased'.

## 411 Cell culture

412 We utilized our previously established cultures of male wild-type and *Kdm5c* knockout (-KO)  
413 embryonic stem cells<sup>42</sup>. Sex was confirmed by genotyping *Uba1/Uba1y* on the X and Y chromo-  
414 somes with the following primers: 5'-TGGATGGTGTGCCAATG-3', 5'-CACCTGCACGTTGCCCTT-  
415 3'. Deletion of *Kdm5c* exons 11 and 12, which destabilize KDM5C protein<sup>12</sup>, was confirmed  
416 through the primers 5'-ATGCCCATATTAAGAGTCCCTG-3', 5'-TCTGCCTTGATGGACTGTT-3', and  
417 5'-GGTTCTAACACTCACATAGTG-3'.

418 Embryonic stem cells (ESCs) and epiblast-like cells were cultured using previously established  
419 methods<sup>38</sup>. Briefly, ESCs were initially cultured in primed ESC (pESC) media consisting of KnockOut  
420 DMEM (Gibco#10829–018), fetal bovine serum (Gibco#A5209501), KnockOut serum replacement  
421 (Invitrogen#10828–028), Glutamax (Gibco#35050-061), Anti-Anti (Gibco#15240-062), MEM Non-essential  
422 amino acids (Gibco#11140-050), and beta-mercaptoethanol (Sigma#M7522). They were then transitioned  
423 into ground-state, "naïve" ESCs (nESCs) by culturing for four passages in N2B27 media containing  
424 DMEM/F12 (Gibco#11330–032), Neurobasal media (Gibco#21103–049), Gluamax (Gibco#35050-061),  
425 Anti-Anti (Gibco#15240-062), N2 supplement (Invitrogen#17502048), and B27 supplement without vitamin  
426 A (Invitrogen#12587-010), and beta-mercaptoethanol (Sigma#M7522). Both pESC and nESC media  
427 were supplemented with 3  $\mu$ M GSK3 inhibitor CHIR99021 (Sigma #SML1046-5MG), 1  $\mu$ M MEK inhibitor  
428 PD0325901 (Sigma #PZ0162-5MG), and 1,000 units/mL leukemia inhibitory factor (LIF, Millipore#ESG1107).

429 nESCs were differentiated into epiblast-like cells (EpiLCs, 48 hours) and extendend EpiLCs (exEpiLCs,  
430 96 hours) by culturing in N2B27 media containing DMEM/F12, Neurobasal media, Gluamax, Anti-Anti, N2  
431 supplement, B27 supplement (Invitrogen#17504044), and beta-mercaptoethanol supplemented with 10  
432 ng/mL fibroblast growth factor 2 (FGF2, R&D Biotechne 233-FB), and 20 ng/mL activin A (R&D Biotechne  
433 338AC050CF), as previously described<sup>38</sup>.

434 **Real time quantitative PCR (RT-qPCR)**

435 nESCs were differentiated into EpiLCs as described above. Cells were lysed with Tri-reagent BD (Sigma  
436 #T3809) at 0, 24, and 48 hours of differentiation. RNA was phase separated with 0.1 uL/uL 1-bromo-3-  
437 chloropropane (Sigma #B9673) and then precipitated with isopropanol (Sigma #I9516) and ethanol puri-  
438 fied. For each sample, 2  $\mu$ g of RNA was reverse transcribed using the ProtoScript II Reverse transcriptase kit  
439 from New England Biolabs (NEB #M0368S) and primed with oligo dT. Expression of *Kdm5c* was detected us-  
440 ing the primers 5'-CCCATGGAGGCCAGAGAATAAG-3' 5'-CTCAGCGGATAAGAGAATTGCTAC-3' and nor-  
441 malized to TBP using the primers 5'-TTCAGAGGATGCTCTAGGGAAGA-3' 5'-CTGTGGAGTAAGTCCTGTGCC-  
442 3' with the Power SYBR™ Green PCR Master Mix (ThermoFisher #4367659).

443 **Western Blot**

444 Total protein was extracted during nESC to EpiLC differentiation at 0, 24, and 48 hours by sonicating cells  
445 at 20% amplitude for 15 seconds in 2X SDS sample buffer, then boiling at 100 °C for 10 minutes. Proteins  
446 were separated on a 7.5% SDS page gel, transferred overnight onto a fluorescent membrane, blotted for  
447 rabbit anti-KDM5C (in house, 1:500) and mouse anti-DAXX (Santa Cruz #(H-7): sc-8043, 1:500) and imaged  
448 using the LiCor Odyssey CLx system. Band intensity was quantified using ImageJ.

449 **RNA sequencing (RNA-seq) data analysis**

450 After ensuring read quality via FastQC (v0.11.8), reads were then mapped to the mm10 *Mus musculus*  
451 genome (Gencode) using STAR (v2.5.3a), during which we removed duplicates and kept only uniquely  
452 mapped reads. Count files were generated by FeatureCounts (Subread v1.5.0), and BAM files were  
453 converted to bigwigs using deeptools (v3.1.3) and visualized by the UCSC genome browser<sup>69</sup>. RStudio  
454 (v3.6.0) was then used to analyze counts files by DESeq2 (v1.26.0)<sup>24</sup> to identify differentially expressed  
455 genes (DEGs) with a q-value (p-adjusted via FDR/Benjamini–Hochberg correction) less than 0.1 and a log2  
456 fold change greater than 0.5. For all DESeq2 analyses, log2 fold changes were calculated with IfcShrink  
457 using the ashR package<sup>90</sup>. MA-plots were generated by ggpibr (v0.6.0), and Eulerr diagrams were generated  
458 by eulerr (v6.1.1). Boxplots and scatterplots were generated by ggpibr (v0.6.0) and ggplot2 (v3.3.2). The  
459 Upset plot was generated via the package UpSetR (v1.4.0)<sup>91</sup>. Gene ontology (GO) analyses were performed  
460 by the R package enrichPlot (v1.16.2) using the biological processes setting and compareCluster.

461 **Chromatin immunoprecipitation followed by DNA sequencing (ChIP-seq) data analysis**

462 ChIP-seq reads were aligned to mm10 using Bowtie1 (v1.1.2) allowing up to two mismatches. Only  
463 uniquely mapped reads were used for analysis. Peaks were called using MACS2 software (v2.2.9.1) using  
464 input BAM files for normalization, with filters for a q-value < 0.1 and a fold enrichment > 1. We removed

465 “black-listed” genomic regions that often give aberrant signals. Common peak sets were obtained in R via  
466 DiffBind<sup>92</sup> (v3.6.5). In the case of KDM5C ChIP-seq, *Kdm5c*-KO peaks false-positive peaks were then  
467 removed from wild-type samples using bedtools (v2.25.0). Peak proximity to genomic loci was determined  
468 by ChIPSeeker<sup>93</sup> (v1.32.1). Gene ontology (GO) analyses were performed by the R package enrichPlot  
469 (v1.16.2) using the biological processes setting and compareCluster. Enriched motifs were identified using  
470 HOMER<sup>60</sup> to search for known motifs within 500 base pairs of the transcription start site. Average binding  
471 across genes was visualized using deeptools (v3.1.3). Bigwigs were visualized using the UCSC genome  
472 browser<sup>69</sup>.

### 473 CpG island (CGI) analysis

474 Locations of CpG islands were determined through the mm10 UCSC genome browser CpG island track<sup>69</sup>,  
475 which classified CGIs as regions that have greater than 50% GC content, are larger than 200 base pairs,  
476 and have a ratio of CG dinucleotides observed over the expected amount greater than 0.6. CGI genomic  
477 coordinates were then annotated using ChIPseeker<sup>93</sup> (v1.32.1) and filtered for ones that lie within promoters  
478 of germline-enriched genes (TSS ± 500).

### 479 Whole genome bisulfite sequencing (WGBS)

480 Genomic DNA (gDNA) from naïve ESCs and extended EpiLCs was extracted using the Wizard Genomic  
481 DNA Purification Kit (Promega A1120), following the instructions for Tissue Culture Cells. gDNA from  
482 two wild-types and two *Kdm5c*-KOs of each cell type was sent to Novogene for WGBS using the Illumina  
483 NovaSeq X Plus platform and sequenced for 150bp paired-end reads (PE150). All samples had greater  
484 than 99% bisulfite conversion rates. Reads were adapter and quality trimmed with Trim Galore (v0.6.10)  
485 and aligned to the mm10 genome using Bismark<sup>94</sup> (v0.22.1). Analysis of differential methylation at germline  
486 gene promoters was performed using methylKit<sup>70</sup> (v1.28.0) with a minimum coverage of 3 paired reads, a  
487 percentage greater than 25% or less than -25%, and q-value less than 0.01. methylKit was also used to  
488 calculate average percentage methylation at germline gene promoters. Methylation bedgraph tracks were  
489 generated via Bismark and visualized using the UCSC genome browser<sup>69</sup>.

### 490 Data availability

#### 491 WGBS in wild-type and *Kdm5c*-KO ESCs and exEpiLCs

492 Raw fastq files are deposited in the Sequence Read Archive (SRA) <https://www.ncbi.nlm.nih.gov/sra>  
493 under the bioProject XXX

494 **Published datasets**

495 All published datasets are available at the Gene Expression Omnibus (GEO) <https://www.ncbi.nlm.nih.gov/geo>. Published RNA-seq datasets analyzed in this study included the male wild-type and *Kdm5c*-KO  
496 adult amygdala and hippocampus<sup>22</sup> (available at GEO: GSE127722). Male and female wild-type, *Kdm5c*-KO,  
497 and *Kdm5c*-HET EpiLCs<sup>42</sup> are available at GEO: GSE96797.

498 Previously published ChIP-seq experiments included KDM5C binding in wild-type and *Kdm5c*-KO  
499 EpiLCs<sup>42</sup> (available at GEO: GSE96797) and mouse primary neuron cultures (PNCs) from the cortex  
500 and hippocampus<sup>12</sup> (available at GEO: GSE61036). ChIP-seq of histone 3 lysine 4 dimethylation (H3K4me2)  
501 in male wild-type and *Kdm5c*-KO EpiLCs<sup>42</sup> is also available at GEO: GSE96797. ChIP-seq of histone 3 lysine  
502 4 trimethylation (H3K4me3) in wild-type and *Kdm5c*-KO male amygdala<sup>22</sup> are available at GEO: GSE127817.  
503

504 **Data analysis**

505 Scripts used to generate the results, tables, and figures of this study are available via the GitHub  
506 repository: XXX

507 **Acknowledgements**

508 We thank Drs. Sundeep Kalantry, Milan Samanta, and Rebecca Malcore for providing protocols and  
509 expertise in culturing mouse ESCs and EpiLCs, as well as providing the wild-type and *Kdm5c*-KO ESCs  
510 used in this study. We thank Dr. Jacob Mueller for his insight in germline gene regulation and directing us to  
511 the germline-depleted mouse models. We also thank Drs. Gabriel Corfas, Kenneth Kwan, Natalie Tronson,  
512 Michael Sutton, Stephanie Bielas, Donna Martin, and the members of the Iwase, Sutton, Bielas, and Martin  
513 labs for helpful discussions and critiques of the data. We thank members of the University of Michigan  
514 Reproductive Sciences Program for providing feedback throughout the development of this work. This work  
515 was supported by grants from the National Institutes of Health (NIH) (National Institute of Neurological  
516 Disorders and Stroke: NS089896, 5R21NS104774, and NS116008 to S.I.), Farrehi Family Foundation Grant  
517 (to S.I.), the University of Michigan Career Training in Reproductive Biology (NIH T32HD079342, to K.M.B.),  
518 the NIH Early Stage Training in the Neurosciences Training Grant (NIH T32NS076401 to K.M.B.), and the  
519 Michigan Predoctoral Training in Genetics Grant (NIH T32GM007544, to I.V.)

520 **Author contributions**

521 K.M.B. and S.I. conceived the study and designed the experiments. I.V. generated the ESC and exEpiLC  
522 WGBS data. K.M.B performed the data analysis and all other experiments. K.M.B and S.I. wrote and edited  
523 the manuscript.

524 **References**

- 525 1. Strahl, B.D., and Allis, C.D. (2000). The language of covalent histone modifications. *Nature* **403**,  
526 41–45. <https://doi.org/10.1038/47412>.
- 527 2. Jenuwein, T., and Allis, C.D. (2001). Translating the Histone Code. *Science* **293**, 1074–1080.  
528 <https://doi.org/10.1126/science.1063127>.
- 529 3. Lewis, E.B. (1978). A gene complex controlling segmentation in *Drosophila*. *Nature* **276**, 565–570.  
530 <https://doi.org/10.1038/276565a0>.
- 531 4. Kennison, J.A., and Tamkun, J.W. (1988). Dosage-dependent modifiers of polycomb and antennapedia  
532 mutations in *Drosophila*. *Proc. Natl. Acad. Sci. U.S.A.* **85**, 8136–8140. <https://doi.org/10.1073/pnas.8>  
5. Kassis, J.A., Kennison, J.A., and Tamkun, J.W. (2017). Polycomb and Trithorax Group Genes in  
534 *Drosophila*. *Genetics* **206**, 1699–1725. <https://doi.org/10.1534/genetics.115.185116>.
- 535 6. Gabriele, M., Lopez Tobon, A., D'Agostino, G., and Testa, G. (2018). The chromatin basis of  
536 neurodevelopmental disorders: Rethinking dysfunction along the molecular and temporal axes. *Prog  
Neuropsychopharmacol Biol Psychiatry* **84**, 306–327. <https://doi.org/10.1016/j.pnpbp.2017.12.013>.
- 537 7. Schaefer, A., Sampath, S.C., Intrator, A., Min, A., Gertler, T.S., Surmeier, D.J., Tarakhovsky, A.,  
538 and Greengard, P. (2009). Control of cognition and adaptive behavior by the GLP/G9a epigenetic  
suppressor complex. *Neuron* **64**, 678–691. <https://doi.org/10.1016/j.neuron.2009.11.019>.
- 539 8. Iwase, S., Lan, F., Bayliss, P., De La Torre-Ubieta, L., Huarte, M., Qi, H.H., Whetstine, J.R., Bonni, A.,  
540 Roberts, T.M., and Shi, Y. (2007). The X-Linked Mental Retardation Gene SMCX/JARID1C Defines a  
Family of Histone H3 Lysine 4 Demethylases. *Cell* **128**, 1077–1088. <https://doi.org/10.1016/j.cell.200>  
7.02.017.
- 541 9. Claes, S., Devriendt, K., Van Goethem, G., Roelen, L., Meireleire, J., Raeymaekers, P., Cassiman,  
542 J.J., and Fryns, J.P. (2000). Novel syndromic form of X-linked complicated spastic paraparesia. *Am J  
Med Genet* **94**, 1–4.
- 543 10. Jensen, L.R., Amende, M., Gurok, U., Moser, B., Gimmel, V., Tzschach, A., Janecke, A.R., Tariverdian,  
544 G., Chelly, J., Fryns, J.P., et al. (2005). Mutations in the JARID1C gene, which is involved in  
transcriptional regulation and chromatin remodeling, cause X-linked mental retardation. *Am J Hum  
Genet* **76**, 227–236. <https://doi.org/10.1086/427563>.
- 545 11. Carmignac, V., Nambot, S., Lehalle, D., Callier, P., Moortgat, S., Benoit, V., Ghoumid, J., Delobel,  
B., Smol, T., Thuillier, C., et al. (2020). Further delineation of the female phenotype with KDM5C  
546 disease causing variants: 19 new individuals and review of the literature. *Clin Genet* **98**, 43–55.  
<https://doi.org/10.1111/cge.13755>.

- 547 12. Iwase, S., Brookes, E., Agarwal, S., Badeaux, A.I., Ito, H., Vallianatos, C.N., Tomassy, G.S., Kasza, T.,  
Lin, G., Thompson, A., et al. (2016). A Mouse Model of X-linked Intellectual Disability Associated with  
Impaired Removal of Histone Methylation. *Cell Reports* *14*, 1000–1009. <https://doi.org/10.1016/j.celrep.2015.12.091>.
- 548
- 549 13. Scandaglia, M., Lopez-Atalaya, J.P., Medrano-Fernandez, A., Lopez-Cascales, M.T., Del Blanco, B.,  
Lipinski, M., Benito, E., Olivares, R., Iwase, S., Shi, Y., et al. (2017). Loss of Kdm5c Causes Spurious  
Transcription and Prevents the Fine-Tuning of Activity-Regulated Enhancers in Neurons. *Cell Rep* *21*,  
47–59. <https://doi.org/10.1016/j.celrep.2017.09.014>.
- 550
- 551 14. Bonefas, K.M., Vallianatos, C.N., Raines, B., Tronson, N.C., and Iwase, S. (2023). Sexually Dimorphic  
Alterations in the Transcriptome and Behavior with Loss of Histone Demethylase KDM5C. *Cells* *12*,  
637. <https://doi.org/10.3390/cells12040637>.
- 552
- 553 15. Devlin, D.K., Ganley, A.R.D., and Takeuchi, N. (2023). A pan-metazoan view of germline-soma  
distinction challenges our understanding of how the metazoan germline evolves. *Current Opinion in  
Systems Biology* *36*, 100486. <https://doi.org/10.1016/j.coisb.2023.100486>.
- 554
- 555 16. Lehmann, R. (2012). Germline Stem Cells: Origin and Destiny. *Cell Stem Cell* *10*, 729–739.  
<https://doi.org/10.1016/j.stem.2012.05.016>.
- 556
- 557 17. Endoh, M., Endo, T.A., Shinga, J., Hayashi, K., Farcas, A., Ma, K.W., Ito, S., Sharif, J., Endoh, T.,  
Onaga, N., et al. (2017). PCGF6-PRC1 suppresses premature differentiation of mouse embryonic  
stem cells by regulating germ cell-related genes. *eLife* *6*. <https://doi.org/10.7554/eLife.21064>.
- 558
- 559 18. Mochizuki, K., Sharif, J., Shirane, K., Uranishi, K., Bogutz, A.B., Janssen, S.M., Suzuki, A., Okuda,  
A., Koseki, H., and Lorincz, M.C. (2021). Repression of germline genes by PRC1.6 and SETDB1  
in the early embryo precedes DNA methylation-mediated silencing. *Nat Commun* *12*, 7020. <https://doi.org/10.1038/s41467-021-27345-x>.
- 560
- 561 19. Borgel, J., Guibert, S., Li, Y., Chiba, H., Schübeler, D., Sasaki, H., Forné, T., and Weber, M. (2010).  
Targets and dynamics of promoter DNA methylation during early mouse development. *Nat Genet* *42*,  
1093–1100. <https://doi.org/10.1038/ng.708>.
- 562
- 563 20. Velasco, G., Hubé, F., Rollin, J., Neuillet, D., Philippe, C., Bouzinba-Segard, H., Galvani, A., Viegas-  
Péquignot, E., and Francastel, C. (2010). Dnmt3b recruitment through E2F6 transcriptional repressor  
mediates germ-line gene silencing in murine somatic tissues. *Proc Natl Acad Sci U S A* *107*, 9281–  
9286. <https://doi.org/10.1073/pnas.1000473107>.
- 564
- 565 21. Hackett, J.A., Reddington, J.P., Nestor, C.E., Dunican, D.S., Branco, M.R., Reichmann, J., Reik,  
W., Surani, M.A., Adams, I.R., and Meehan, R.R. (2012). Promoter DNA methylation couples  
genome-defence mechanisms to epigenetic reprogramming in the mouse germline. *Development*  
139, 3623–3632. <https://doi.org/10.1242/dev.081661>.
- 566

- 567 22. Vallianatos, C.N., Raines, B., Porter, R.S., Bonefas, K.M., Wu, M.C., Garay, P.M., Collette, K.M.,  
Seo, Y.A., Dou, Y., Keegan, C.E., et al. (2020). Mutually suppressive roles of KMT2A and KDM5C  
in behaviour, neuronal structure, and histone H3K4 methylation. *Commun Biol* 3, 278. <https://doi.org/10.1038/s42003-020-1001-6>.
- 568
- 569 23. Li, B., Qing, T., Zhu, J., Wen, Z., Yu, Y., Fukumura, R., Zheng, Y., Gondo, Y., and Shi, L. (2017). A  
570 Comprehensive Mouse Transcriptomic BodyMap across 17 Tissues by RNA-seq. *Sci Rep* 7, 4200.  
<https://doi.org/10.1038/s41598-017-04520-z>.
- 571 24. Love, M.I., Huber, W., and Anders, S. (2014). Moderated estimation of fold change and dispersion for  
572 RNA-seq data with DESeq2. *Genome Biol* 15, 550. <https://doi.org/10.1186/s13059-014-0550-8>.
- 573 25. Crackower, M.A., Kolas, N.K., Noguchi, J., Sarao, R., Kikuchi, K., Kaneko, H., Kobayashi, E., Kawai, Y.,  
Kozieradzki, I., Landers, R., et al. (2003). Essential Role of Fkbp6 in Male Fertility and Homologous  
574 Chromosome Pairing in Meiosis. *Science* 300, 1291–1295. <https://doi.org/10.1126/science.1083022>.
- 575 26. Xiol, J., Cora, E., Koglgruber, R., Chuma, S., Subramanian, S., Hosokawa, M., Reuter, M., Yang, Z.,  
Berninger, P., Palencia, A., et al. (2012). A Role for Fkbp6 and the Chaperone Machinery in piRNA  
576 Amplification and Transposon Silencing. *Molecular Cell* 47, 970–979. <https://doi.org/10.1016/j.molcel.2012.07.019>.
- 577 27. Cheng, S., Altmeppen, G., So, C., Welp, L.M., Penir, S., Ruhwedel, T., Menelaou, K., Harasimov, K.,  
Stützer, A., Blayney, M., et al. (2022). Mammalian oocytes store mRNAs in a mitochondria-associated  
578 membraneless compartment. *Science* 378, eabq4835. <https://doi.org/10.1126/science.abq4835>.
- 579 28. Rouland, A., Masson, D., Lagrost, L., Vergès, B., Gautier, T., and Bouillet, B. (2022). Role of  
580 apolipoprotein C1 in lipoprotein metabolism, atherosclerosis and diabetes: A systematic review.  
*Cardiovasc Diabetol* 21, 272. <https://doi.org/10.1186/s12933-022-01703-5>.
- 581 29. Leduc, V., Jasmin-Bélanger, S., and Poirier, J. (2010). APOE and cholesterol homeostasis in  
582 Alzheimer's disease. *Trends in Molecular Medicine* 16, 469–477. <https://doi.org/10.1016/j.molmed.2010.07.008>.
- 583 30. Mueller, J.L., Skaletsky, H., Brown, L.G., Zaghlul, S., Rock, S., Graves, T., Auger, K., Warren,  
584 W.C., Wilson, R.K., and Page, D.C. (2013). Independent specialization of the human and mouse X  
chromosomes for the male germ line. *Nat Genet* 45, 1083–1087. <https://doi.org/10.1038/ng.2705>.
- 585 31. Handel, M.A., and Eppig, J.J. (1979). Sertoli Cell Differentiation in the Testes of Mice Genetically  
586 Deficient in Germ Cells. *Biology of Reproduction* 20, 1031–1038. <https://doi.org/10.1095/biolreprod20.5.1031>.
- 587 32. Green, C.D., Ma, Q., Manske, G.L., Shami, A.N., Zheng, X., Marini, S., Moritz, L., Sultan, C.,  
Gurczynski, S.J., Moore, B.B., et al. (2018). A Comprehensive Roadmap of Murine Spermatogenesis  
Defined by Single-Cell RNA-Seq. *Dev Cell* 46, 651–667.e10. <https://doi.org/10.1016/j.devcel.2018.07.025>.
- 588

- 589 33. Soh, Y.Q., Junker, J.P., Gill, M.E., Mueller, J.L., van Oudenaarden, A., and Page, D.C. (2015). A  
Gene Regulatory Program for Meiotic Prophase in the Fetal Ovary. *PLoS Genet* *11*, e1005531.  
<https://doi.org/10.1371/journal.pgen.1005531>.
- 590
- 591 34. Magnúsdóttir, E., and Surani, M.A. (2014). How to make a primordial germ cell. *Development* *141*,  
245–252. <https://doi.org/10.1242/dev.098269>.
- 592
- 593 35. Günesdogan, U., Magnúsdóttir, E., and Surani, M.A. (2014). Primordial germ cell specification: A  
context-dependent cellular differentiation event [corrected]. *Philos Trans R Soc Lond B Biol Sci* *369*.  
<https://doi.org/10.1098/rstb.2013.0543>.
- 594
- 595 36. Bardot, E.S., and Hadjantonakis, A.-K. (2020). Mouse gastrulation: Coordination of tissue patterning,  
specification and diversification of cell fate. *Mechanisms of Development* *163*, 103617. <https://doi.org/10.1016/j.mod.2020.103617>.
- 596
- 597 37. Hayashi, K., Ohta, H., Kurimoto, K., Aramaki, S., and Saitou, M. (2011). Reconstitution of the  
mouse germ cell specification pathway in culture by pluripotent stem cells. *Cell* *146*, 519–532.  
<https://doi.org/10.1016/j.cell.2011.06.052>.
- 598
- 599 38. Samanta, M., and Kalantry, S. (2020). Generating primed pluripotent epiblast stem cells: A methodol-  
600 ogy chapter. *Curr Top Dev Biol* *138*, 139–174. <https://doi.org/10.1016/bs.ctdb.2020.01.005>.
- 601 39. Welling, M., Chen, H., Muñoz, J., Musheev, M.U., Kester, L., Junker, J.P., Mischerikow, N., Arbab, M.,  
Kuijk, E., Silberstein, L., et al. (2015). DAZL regulates Tet1 translation in murine embryonic stem cells.  
EMBO Reports *16*, 791–802. <https://doi.org/10.15252/embr.201540538>.
- 602
- 603 40. Macfarlan, T.S., Gifford, W.D., Driscoll, S., Lettieri, K., Rowe, H.M., Bonanomi, D., Firth, A., Singer, O.,  
Trono, D., and Pfaff, S.L. (2012). Embryonic stem cell potency fluctuates with endogenous retrovirus  
604 activity. *Nature* *487*, 57–63. <https://doi.org/10.1038/nature11244>.
- 605 41. Suzuki, A., Hirasaki, M., Hishida, T., Wu, J., Okamura, D., Ueda, A., Nishimoto, M., Nakachi, Y.,  
Mizuno, Y., Okazaki, Y., et al. (2016). Loss of MAX results in meiotic entry in mouse embryonic and  
606 germline stem cells. *Nat Commun* *7*, 11056. <https://doi.org/10.1038/ncomms11056>.
- 607 42. Samanta, M.K., Gayen, S., Harris, C., Maclary, E., Murata-Nakamura, Y., Malcore, R.M., Porter, R.S.,  
Garay, P.M., Vallianatos, C.N., Samollow, P.B., et al. (2022). Activation of Xist by an evolutionarily  
conserved function of KDM5C demethylase. *Nat Commun* *13*, 2602. <https://doi.org/10.1038/s41467-022-30352-1>.
- 608
- 609 43. Koubova, J., Menke, D.B., Zhou, Q., Capel, B., Griswold, M.D., and Page, D.C. (2006). Retinoic  
acid regulates sex-specific timing of meiotic initiation in mice. *Proc. Natl. Acad. Sci. U.S.A.* *103*,  
2474–2479. <https://doi.org/10.1073/pnas.0510813103>.
- 610

- 611 44. Lin, Y., Gill, M.E., Koubova, J., and Page, D.C. (2008). Germ Cell-Intrinsic and -Extrinsic Factors  
612 Govern Meiotic Initiation in Mouse Embryos. *Science* *322*, 1685–1687. <https://doi.org/10.1126/science.1166340>.
- 613 45. Endo, T., Mikedis, M.M., Nicholls, P.K., Page, D.C., and De Rooij, D.G. (2019). Retinoic Acid and Germ  
614 Cell Development in the Ovary and Testis. *Biomolecules* *9*, 775. <https://doi.org/10.3390/biom9120775>.
- 615 46. Gupta, N., Yakhou, L., Albert, J.R., Azogui, A., Ferry, L., Kirsh, O., Miura, F., Battault, S., Yamaguchi,  
616 K., Laisné, M., et al. (2023). A genome-wide screen reveals new regulators of the 2-cell-like cell state.  
*Nat Struct Mol Biol*. <https://doi.org/10.1038/s41594-023-01038-z>.
- 617 47. Pohlers, M., Truss, M., Frede, U., Scholz, A., Strehle, M., Kuban, R.-J., Hoffmann, B., Morkel, M.,  
618 Birchmeier, C., and Hagemeier, C. (2005). A Role for E2F6 in the Restriction of Male-Germ-Cell-  
Specific Gene Expression. *Current Biology* *15*, 1051–1057. <https://doi.org/10.1016/j.cub.2005.04.060>.
- 619 48. Dahlet, T., Truss, M., Frede, U., Al Adhami, H., Bardet, A.F., Dumas, M., Vallet, J., Chicher, J.,  
620 Hammann, P., Kottnik, S., et al. (2021). E2F6 initiates stable epigenetic silencing of germline genes  
during embryonic development. *Nat Commun* *12*, 3582. <https://doi.org/10.1038/s41467-021-23596-w>.
- 621 49. Agulnik, A.I., Mitchell, M.J., Mattei, M.G., Borsani, G., Avner, P.A., Lerner, J.L., and Bishop, C.E.  
622 (1994). A novel X gene with a widely transcribed Y-linked homologue escapes X-inactivation in mouse  
and human. *Hum Mol Genet* *3*, 879–884. <https://doi.org/10.1093/hmg/3.6.879>.
- 623 50. Carrel, L., Hunt, P.A., and Willard, H.F. (1996). Tissue and lineage-specific variation in inactive  
624 X chromosome expression of the murine Smcx gene. *Hum Mol Genet* *5*, 1361–1366. <https://doi.org/10.1093/hmg/5.9.1361>.
- 625 51. Sheardown, S., Norris, D., Fisher, A., and Brockdorff, N. (1996). The mouse Smcx gene exhibits  
developmental and tissue specific variation in degree of escape from X inactivation. *Hum Mol Genet*  
626 *5*, 1355–1360. <https://doi.org/10.1093/hmg/5.9.1355>.
- 627 52. Xu, J., Deng, X., and Disteche, C.M. (2008). Sex-Specific Expression of the X-Linked Histone  
Demethylase Gene Jarid1c in Brain. *PLoS ONE* *3*, e2553. <https://doi.org/10.1371/journal.pone.0002553>.
- 629 53. Wang, P.J., McCarrey, J.R., Yang, F., and Page, D.C. (2001). An abundance of X-linked genes  
630 expressed in spermatogonia. *Nat Genet* *27*, 422–426. <https://doi.org/10.1038/86927>.
- 631 54. Khil, P.P., Smirnova, N.A., Romanienko, P.J., and Camerini-Otero, R.D. (2004). The mouse X  
chromosome is enriched for sex-biased genes not subject to selection by meiotic sex chromosome  
inactivation. *Nat Genet* *36*, 642–646. <https://doi.org/10.1038/ng1368>.

- 633 55. Al Adhami, H., Vallet, J., Schaal, C., Schumacher, P., Bardet, A.F., Dumas, M., Chicher, J., Hammann, P., Daujat, S., and Weber, M. (2023). Systematic identification of factors involved in the silencing of germline genes in mouse embryonic stem cells. *Nucleic Acids Research* *51*, 3130–3149. <https://doi.org/10.1093/nar/gkad071>.
- 634
- 635 56. Hurlin, P.J. (1999). Mga, a dual-specificity transcription factor that interacts with Max and contains a T-domain DNA-binding motif. *The EMBO Journal* *18*, 7019–7028. <https://doi.org/10.1093/emboj/18.24.7019>.
- 636
- 637 57. Tatsumi, D., Hayashi, Y., Endo, M., Kobayashi, H., Yoshioka, T., Kiso, K., Kanno, S., Nakai, Y., Maeda, I., Mochizuki, K., et al. (2018). DNMTs and SETDB1 function as co-repressors in MAX-mediated repression of germ cell-related genes in mouse embryonic stem cells. *PLoS ONE* *13*, e0205969. <https://doi.org/10.1371/journal.pone.0205969>.
- 638
- 639 58. Stielow, B., Finkernagel, F., Stiewe, T., Nist, A., and Suske, G. (2018). MGA, L3MBTL2 and E2F6 determine genomic binding of the non-canonical Polycomb repressive complex PRC1.6. *PLoS Genet* *14*, e1007193. <https://doi.org/10.1371/journal.pgen.1007193>.
- 640
- 641 59. Tahiliani, M., Mei, P., Fang, R., Leonor, T., Rutenberg, M., Shimizu, F., Li, J., Rao, A., and Shi, Y. (2007). The histone H3K4 demethylase SMCX links REST target genes to X-linked mental retardation. *Nature* *447*, 601–605. <https://doi.org/10.1038/nature05823>.
- 642
- 643 60. Heinz, S., Benner, C., Spann, N., Bertolino, E., Lin, Y.C., Laslo, P., Cheng, J.X., Murre, C., Singh, H., and Glass, C.K. (2010). Simple Combinations of Lineage-Determining Transcription Factors Prime cis-Regulatory Elements Required for Macrophage and B Cell Identities. *Molecular Cell* *38*, 576–589. <https://doi.org/10.1016/j.molcel.2010.05.004>.
- 644
- 645 61. Gajiwala, K.S., Chen, H., Cornille, F., Roques, B.P., Reith, W., Mach, B., and Burley, S.K. (2000). Structure of the winged-helix protein hRFX1 reveals a new mode of DNA binding. *Nature* *403*, 916–921. <https://doi.org/10.1038/35002634>.
- 646
- 647 62. Swoboda, P., Adler, H.T., and Thomas, J.H. (2000). The RFX-Type Transcription Factor DAF-19 Regulates Sensory Neuron Cilium Formation in *C. elegans*. *Molecular Cell* *5*, 411–421. [https://doi.org/10.1016/S1097-2765\(00\)80436-0](https://doi.org/10.1016/S1097-2765(00)80436-0).
- 648
- 649 63. Ashique, A.M., Choe, Y., Karlen, M., May, S.R., Phamluong, K., Solloway, M.J., Ericson, J., and Peterson, A.S. (2009). The Rfx4 Transcription Factor Modulates Shh Signaling by Regional Control of Ciliogenesis. *Sci. Signal.* *2*. <https://doi.org/10.1126/scisignal.2000602>.
- 650
- 651 64. Kistler, W.S., Baas, D., Lemeille, S., Paschaki, M., Seguin-Estevez, Q., Barras, E., Ma, W., Duteyrat, J.-L., Morlé, L., Durand, B., et al. (2015). RFX2 Is a Major Transcriptional Regulator of Spermiogenesis. *PLoS Genet* *11*, e1005368. <https://doi.org/10.1371/journal.pgen.1005368>.
- 652

- 653 65. Wu, Y., Hu, X., Li, Z., Wang, M., Li, S., Wang, X., Lin, X., Liao, S., Zhang, Z., Feng, X., et al.  
654 (2016). Transcription Factor RFX2 Is a Key Regulator of Mouse Spermiogenesis. *Sci Rep* 6, 20435.  
<https://doi.org/10.1038/srep20435>.
- 655 66. Otani, J., Nankumo, T., Arita, K., Inamoto, S., Ariyoshi, M., and Shirakawa, M. (2009). Structural basis  
656 for recognition of H3K4 methylation status by the DNA methyltransferase 3A ATRX–DNMT3–DNMT3L  
657 domain. *EMBO Reports* 10, 1235–1241. <https://doi.org/10.1038/embor.2009.218>.
- 658 67. Guo, X., Wang, L., Li, J., Ding, Z., Xiao, J., Yin, X., He, S., Shi, P., Dong, L., Li, G., et al. (2015).  
Structural insight into autoinhibition and histone H3-induced activation of DNMT3A. *Nature* 517,  
640–644. <https://doi.org/10.1038/nature13899>.
- 659 68. Meissner, A., Mikkelsen, T.S., Gu, H., Wernig, M., Hanna, J., Sivachenko, A., Zhang, X., Bernstein,  
660 B.E., Nusbaum, C., Jaffe, D.B., et al. (2008). Genome-scale DNA methylation maps of pluripotent and  
differentiated cells. *Nature* 454, 766–770. <https://doi.org/10.1038/nature07107>.
- 661 69. Nassar, L.R., Barber, G.P., Benet-Pagès, A., Casper, J., Clawson, H., Diekhans, M., Fischer, C.,  
Gonzalez, J.N., Hinrichs, A.S., Lee, B.T., et al. (2023). The UCSC Genome Browser database: 2023  
662 update. *Nucleic Acids Research* 51, D1188–D1195. <https://doi.org/10.1093/nar/gkac1072>.
- 663 70. Akalin, A., Kormaksson, M., Li, S., Garrett-Bakelman, F.E., Figueiroa, M.E., Melnick, A., and Mason,  
C.E. (2012). methylKit: A comprehensive R package for the analysis of genome-wide DNA methylation  
664 profiles. *Genome Biol* 13, R87. <https://doi.org/10.1186/gb-2012-13-10-r87>.
- 665 71. Torres-Padilla, M.-E. (2020). On transposons and totipotency. *Philos Trans R Soc Lond B Biol Sci*  
666 375, 20190339. <https://doi.org/10.1098/rstb.2019.0339>.
- 667 72. Yang, M., Yu, H., Yu, X., Liang, S., Hu, Y., Luo, Y., Izsvák, Z., Sun, C., and Wang, J. (2022). Chemical-  
induced chromatin remodeling reprograms mouse ESCs to totipotent-like stem cells. *Cell Stem Cell*  
668 29, 400–418.e13. <https://doi.org/10.1016/j.stem.2022.01.010>.
- 669 73. Zhang, J., Zhang, M., Acampora, D., Vojtek, M., Yuan, D., Simeone, A., and Chambers, I. (2018).  
OTX2 restricts entry to the mouse germline. *Nature* 562, 595–599. [018-0581-5](https://doi.org/10.1038/s41586-<br/>670 018-0581-5).
- 671 74. Weber, M., Hellmann, I., Stadler, M.B., Ramos, L., Pääbo, S., Rebhan, M., and Schübeler, D. (2007).  
Distribution, silencing potential and evolutionary impact of promoter DNA methylation in the human  
672 genome. *Nat Genet* 39, 457–466. <https://doi.org/10.1038/ng1990>.
- 673 75. Aubert, Y., Egolf, S., and Capell, B.C. (2019). The Unexpected Noncatalytic Roles of Histone Modifiers  
in Development and Disease. *Trends in Genetics* 35, 645–657. <https://doi.org/10.1016/j.tig.2019.06.004>.

- 675 76. Morgan, M.A.J., and Shilatifard, A. (2020). Reevaluating the roles of histone-modifying enzymes  
and their associated chromatin modifications in transcriptional regulation. *Nat Genet* 52, 1271–1281.  
<https://doi.org/10.1038/s41588-020-00736-4>.
- 676
- 677 77. Long, H.K., King, H.W., Patient, R.K., Odom, D.T., and Klose, R.J. (2016). Protection of CpG  
islands from DNA methylation is DNA-encoded and evolutionarily conserved. *Nucleic Acids Res* 44,  
6693–6706. <https://doi.org/10.1093/nar/gkw258>.
- 678
- 679 78. Abildayeva, K., Berbée, J.F.P., Blokland, A., Jansen, P.J., Hoek, F.J., Meijer, O., Lütjohann, D., Gautier,  
T., Pillot, T., De Vente, J., et al. (2008). Human apolipoprotein C-I expression in mice impairs learning  
and memory functions. *Journal of Lipid Research* 49, 856–869. <https://doi.org/10.1194/jlr.M700518JLR200>.
- 680
- 681 79. Wang, D., Kennedy, S., Conte, D., Kim, J.K., Gabel, H.W., Kamath, R.S., Mello, C.C., and Ruvkun,  
G. (2005). Somatic misexpression of germline P granules and enhanced RNA interference in  
retinoblastoma pathway mutants. *Nature* 436, 593–597. <https://doi.org/10.1038/nature04010>.
- 682
- 683 80. Wu, X., Shi, Z., Cui, M., Han, M., and Ruvkun, G. (2012). Repression of germline RNAi pathways  
in somatic cells by retinoblastoma pathway chromatin complexes. *PLoS Genet* 8, e1002542. <https://doi.org/10.1371/journal.pgen.1002542>.
- 684
- 685 81. Nielsen, A.Y., and Gjerstorff, M.F. (2016). Ectopic Expression of Testis Germ Cell Proteins in Cancer  
and Its Potential Role in Genomic Instability. *Int J Mol Sci* 17. <https://doi.org/10.3390/ijms17060890>.
- 686
- 687 82. Adebayo Babatunde, K., Najafi, A., Salehipour, P., Modarressi, M.H., and Mobasheri, M.B. (2017).  
Cancer/Testis genes in relation to sperm biology and function. *Iranian Journal of Basic Medical  
Sciences* 20. <https://doi.org/10.22038/ijbms.2017.9259>.
- 688
- 689 83. Janic, A., Mendizabal, L., Llamazares, S., Rossell, D., and Gonzalez, C. (2010). Ectopic expression  
of germline genes drives malignant brain tumor growth in *Drosophila*. *Science* 330, 1824–1827.  
<https://doi.org/10.1126/science.1195481>.
- 690
- 691 84. Ghafouri-Fard, S., and Modarressi, M.-H. (2012). Expression of Cancer–Testis Genes in Brain Tumors:  
Implications for Cancer Immunotherapy. *Immunotherapy* 4, 59–75. <https://doi.org/10.2217/imt.11.145>.
- 692
- 693 85. Nin, D.S., and Deng, L.-W. (2023). Biology of Cancer-Testis Antigens and Their Therapeutic Implications  
in Cancer. *Cells* 12, 926. <https://doi.org/10.3390/cells12060926>.
- 694
- 695 86. Bonefas, K.M., and Iwase, S. (2021). Soma-to-germline transformation in chromatin-linked neurode-  
velopmental disorders? *FEBS J.* <https://doi.org/10.1111/febs.16196>.
- 696
- 697 87. Velasco, G., Walton, E.L., Sterlin, D., Hédouin, S., Nitta, H., Ito, Y., Fouyssac, F., Mégarbané, A.,  
Sasaki, H., Picard, C., et al. (2014). Germline genes hypomethylation and expression define a  
molecular signature in peripheral blood of ICF patients: Implications for diagnosis and etiology.  
*Orphanet J Rare Dis* 9, 56. <https://doi.org/10.1186/1750-1172-9-56>.
- 698

- 699 88. Walton, E.L., Francastel, C., and Velasco, G. (2014). Dnmt3b Prefers Germ Line Genes and Cen-  
700 tromeric Regions: Lessons from the ICF Syndrome and Cancer and Implications for Diseases. *Biology*  
(Basel) 3, 578–605. <https://doi.org/10.3390/biology3030578>.
- 701 89. Graham-Paquin, A.-L., Saini, D., Sirois, J., Hossain, I., Katz, M.S., Zhuang, Q.K.-W., Kwon, S.Y.,  
Yamanaka, Y., Bourque, G., Bouchard, M., et al. (2023). ZMYM2 is essential for methylation of  
germline genes and active transposons in embryonic development. *Nucleic Acids Research*, gkad540.  
702 <https://doi.org/10.1093/nar/gkad540>.
- 703 90. Stephens, M. (2016). False discovery rates: A new deal. *Biostat*, kxw041. <https://doi.org/10.1093/biostatistics/kxw041>.
- 704 91. Conway, J.R., Lex, A., and Gehlenborg, N. (2017). UpSetR: An R package for the visualization of  
intersecting sets and their properties. *Bioinformatics* 33, 2938–2940. <https://doi.org/10.1093/bioinformatics/btx364>.
- 705 92. Ross-Innes, C.S., Stark, R., Teschendorff, A.E., Holmes, K.A., Ali, H.R., Dunning, M.J., Brown, G.D.,  
706 Gojis, O., Ellis, I.O., Green, A.R., et al. (2012). Differential oestrogen receptor binding is associated  
with clinical outcome in breast cancer. *Nature* 481, 389–393. <https://doi.org/10.1038/nature10730>.
- 707 93. Yu, G., Wang, L.G., and He, Q.Y. (2015). ChIPseeker: An R/Bioconductor package for ChIP peak  
708 annotation, comparison and visualization. *Bioinformatics* 31, 2382–2383. <https://doi.org/10.1093/bioinformatics/btv145>.
- 709 94. Krueger, F., and Andrews, S.R. (2011). Bismark: A flexible aligner and methylation caller for Bisulfite-  
710 Seq applications. *Bioinformatics* 27, 1571–1572. <https://doi.org/10.1093/bioinformatics/btr167>.
- 711 712

713 **Figures and Tables**

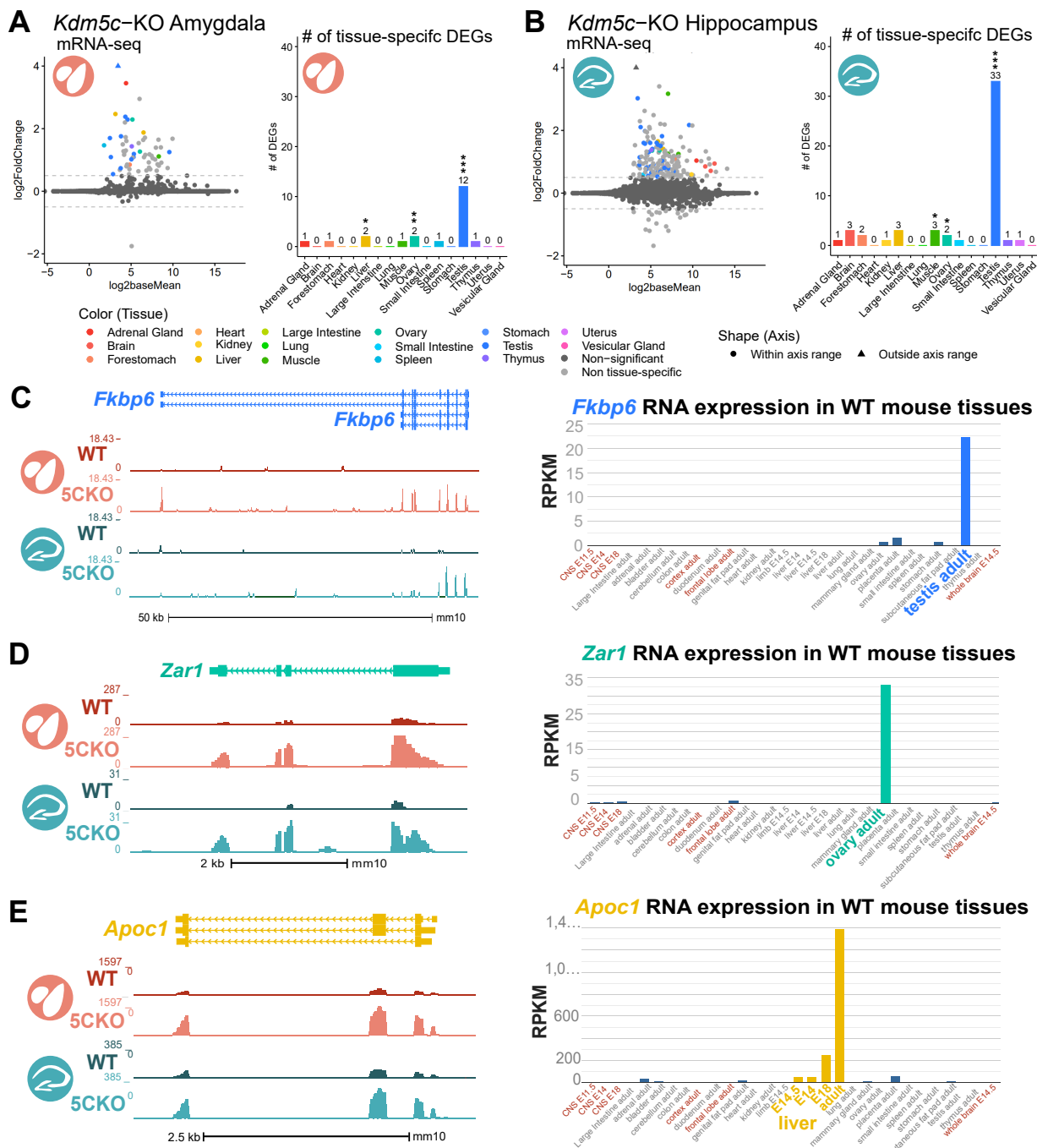


**Figure 1: Tissue-enriched genes are misexpressed in the *Kdm5c*-KO brain.** **A-B.** Expression of tissue-enriched genes (Li et al 2017) in the male *Kdm5c*-KO amygdala (A) and hippocampus (B). Left - MA plot of mRNA-sequencing. Right - Number of tissue-enriched differentially expressed genes (DEGs). \*  $p < 0.05$ , \*\*  $p < 0.01$ , \*\*\*  $p < 0.001$ , Fisher's exact test. **C.** Left - UCSC browser view of an example aberrantly expressed testis-enriched DEG, *FK506 binding protein 6* (*Fkbp6*) in the wild-type (WT) and *Kdm5c*-KO (5CKO) amygdala (red) and hippocampus (teal) (Average,  $n = 4$ ). Right - Expression of *Cyct* in wild-type tissues from NCBI Gene, with testis highlighted in blue and brain tissues highlighted in red. **D.** Left - UCSC browser view of an example ovary-enriched DEG, *Zygotic arrest 1* (*Zar1*). Right - Expression of *Zar1* in wild-type tissues from NCBI Gene, with ovary highlighted in teal and brain tissues highlighted in red. **E.** Left - UCSC browser view of an example liver-enriched DEG, *Apolipoprotein C-I* (*Apoc1*). Right - Expression of *Apoc1* in wild-type tissues from NCBI Gene, with liver highlighted in orange and brain tissues highlighted in red.

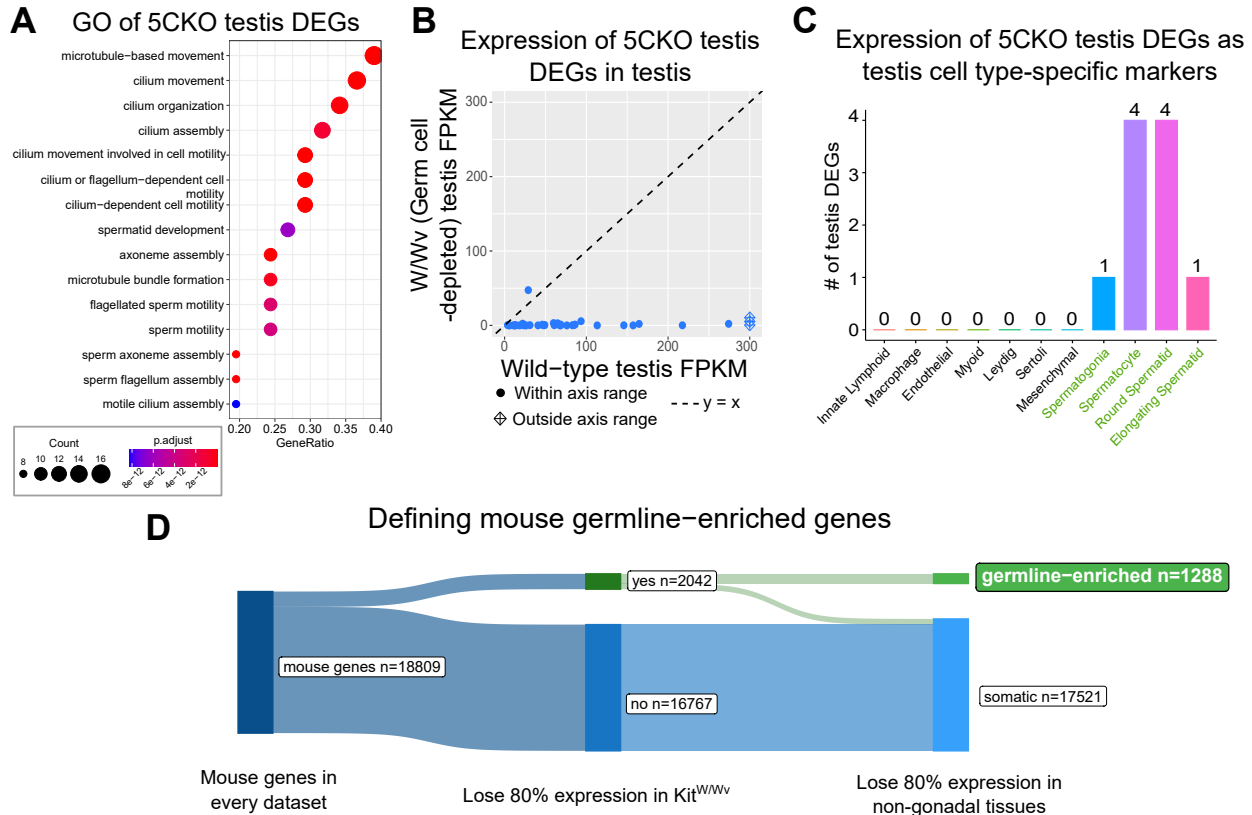


**Figure 2: Aberrant transcription of germline genes in the *Kdm5c*-KO in the brain.** **A.** enrichPlot gene ontology (GO) of *Kdm5c*-KO amygdala and hippocampus testis-enriched DEGs **B.** Expression of testis DEGs in wild-type (WT) testis versus germ cell-depleted (W/Wv) testis (Mueller et al 2013). Expression is in Fragments Per Kilobase of transcript per Million mapped reads (FPKM). **C.** Number of testis DEGs that were classified as cell-type specific markers in a single cell RNA-seq dataset of the testis (Green et al 2018). Germline cell types are highlighted in green, somatic cell types in black. **D.** Sankey diagram of mouse genes filtered for germline enrichment based on their expression in wild-type and W/Wv mice and in adult mouse non-gonadal tissues (Li et al 2017).

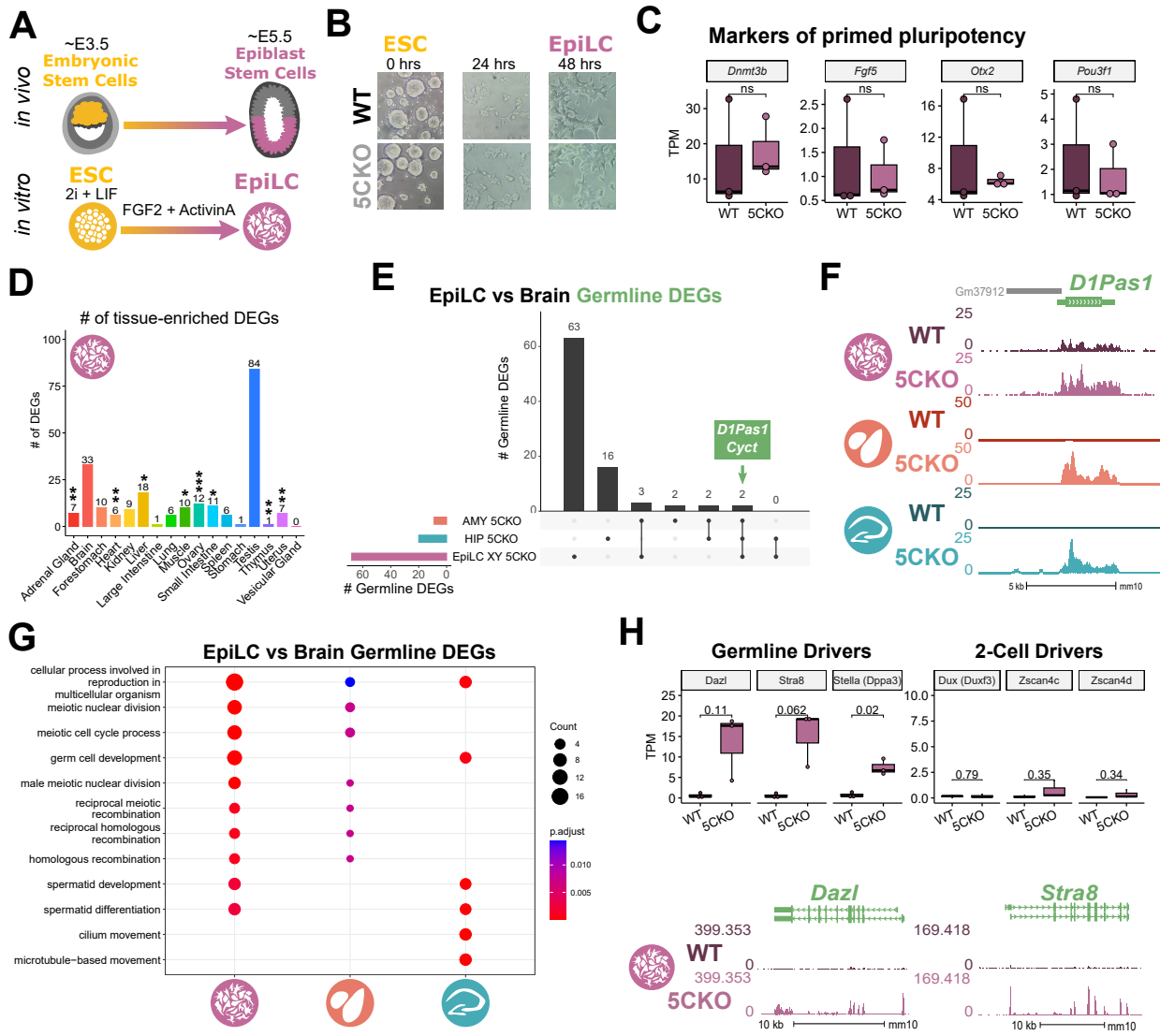


**Figure 3: Kdm5c-KO epiblast-like cells express key drivers of germline identity** **A.** Top - Diagram of *in vivo* differentiation of embryonic stem cells (ESCs) of the inner cell mass into epiblast stem cells. Bottom - *in vitro* differentiation of ESCs into epiblast-like cells (EpiLCs). **B.** Representative images of male wild-type (WT) and *Kdm5c*-KO (5CKO) cells during ESC to EpiLC differentiation. Brightfield images taken at 20X. **C.** No significant difference in primed pluripotency marker expression in wild-type versus *Kdm5c*-KO EpiLCs. Welch's t-test, expression in transcripts per million (TPM). **D.** Number of tissue-enriched differentially expressed genes (DEGs) in *Kdm5c*-KO EpiLCs. \*  $p < 0.05$ , \*\*  $p < 0.01$ , \*\*\*  $p < 0.001$ , Fisher's exact test. **E.** Upset plot displaying the overlap of germline DEGs expressed in *Kdm5c*-KO EpiLCs, amygdala (AMY), and hippocampus (HIP) RNA-seq datasets. **F.** UCSC browser view of an example germline gene, *D1Pas1*, that is dysregulated *Kdm5c*-KO EpiLCs (top, purple. Average,  $n = 3$ ), amygdala (middle, red. Average,  $n = 4$ ), and hippocampus (bottom, blue. Average,  $n = 4$ ). **G.** enrichPlot gene ontology analysis comparing enriched biological processes for *Kdm5c*-KO EpiLC, amygdala, and hippocampus germline DEGs. **H.** Top left - Example germline identity DEGs unique to EpiLCs. Top right - Example 2-cell genes that are not dysregulated in *Kdm5c*-KO EpiLCs. p-values for Welch's t-test. Bottom - UCSC browser view of *Dazl* and *Stra8* expression in wild-type and *Kdm5c*-KO EpiLCs (Average,  $n = 3$ ).

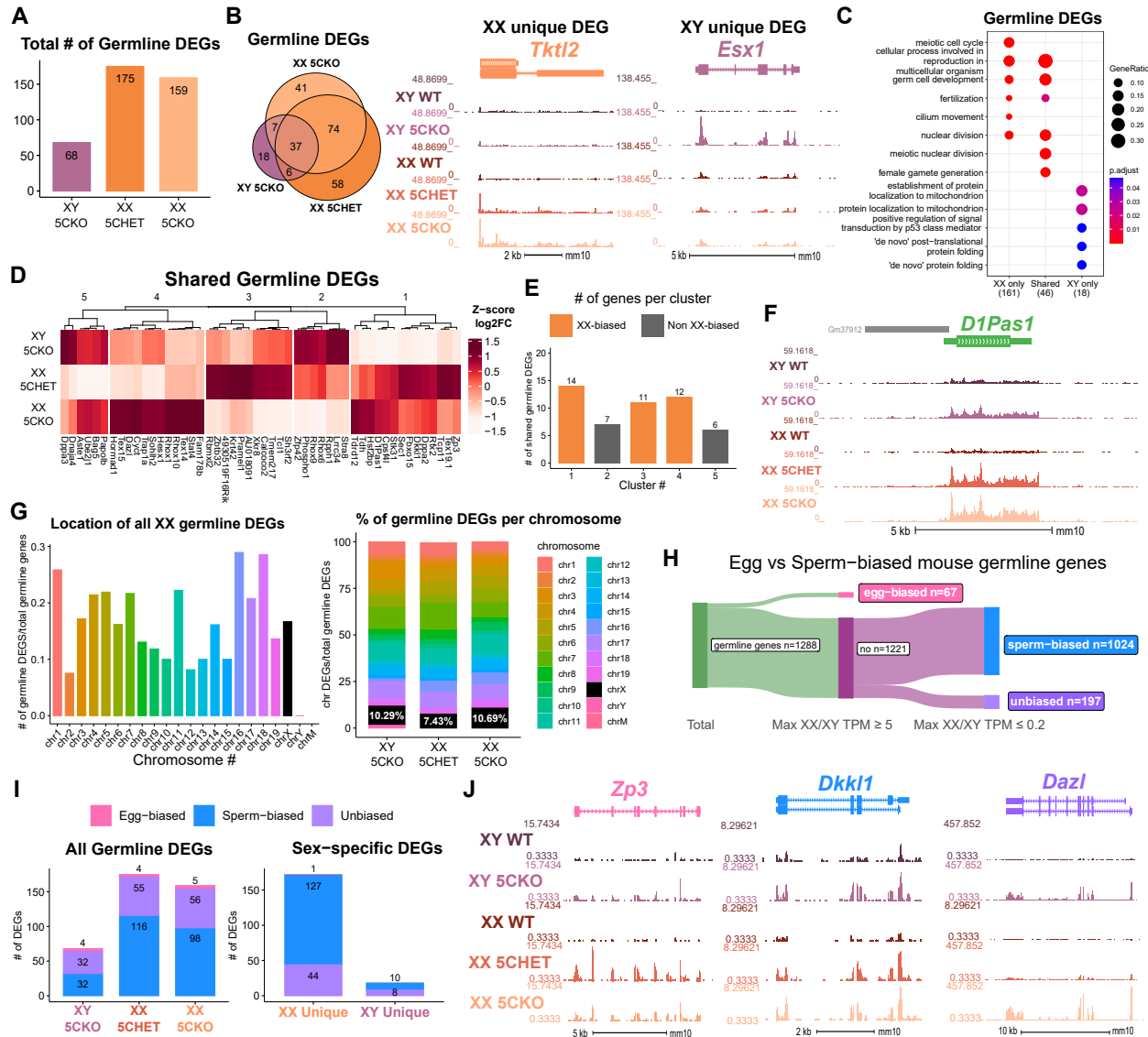


**Figure 4: Chromosomal sex influences *Kdm5c*-KO germline gene misexpression.** **A.** Total number of germline-enriched RNA-seq DEGs for male hemizygous *Kdm5c* knockout EpilCs (XY 5CKO, purple), female heterozygous *Kdm5c* knockout (XX 5CHET, orange), female homozygous *Kdm5c* knockout (XX 5CKO, light orange) EpilCs. **B.** Left - Eulerr overlap of *Kdm5c* mutant male and female EpilC germline DEGs. Right - Example of germline DEGs unique to females or males, *Tktl2* and *Esx1*. **C.** enrichPlot gene ontology analysis comparing enriched biological processes for germline DEGs shared between *Kdm5c* mutant males and females, or unique to one sex (XX only or XY only). **D.** Heatmap of germline DEGs shared between male and female mutants. Color is the average log 2 fold change from sex-matched wild-type, z-scored across rows. **E.** Number of genes within each cluster from D. Clusters with higher expression in females compared to males (XX-biased) highlighted in orange. **F.** UCSC browser view of a male and female shared germline DEG *D1Pas1* that is more highly expressed in female mutants (Average, n = 3). **G.** Left - Number of all female germline DEGs located on each chromosome over the total number of germline-enriched genes on that chromosome. Right - Percentage of germline DEGs that lie on each chromosome for each *Kdm5c* mutant. X chromosome highlighted in black. **H.** Sankey diagram classifying egg-biased (pink) and sperm-biased (blue) and unbiased (purple) mouse germline-enriched genes. **I.** Number of egg, sperm, or unbiased germline DEGs for male and female *Kdm5c* mutants. **J.** UCSC browser view of egg-biased (*Zp3*), sperm-biased (*Dkk1*), and unbiased (*Dazl*) germline genes dysregulated in both male and female *Kdm5c* mutants (Average of n = 3).

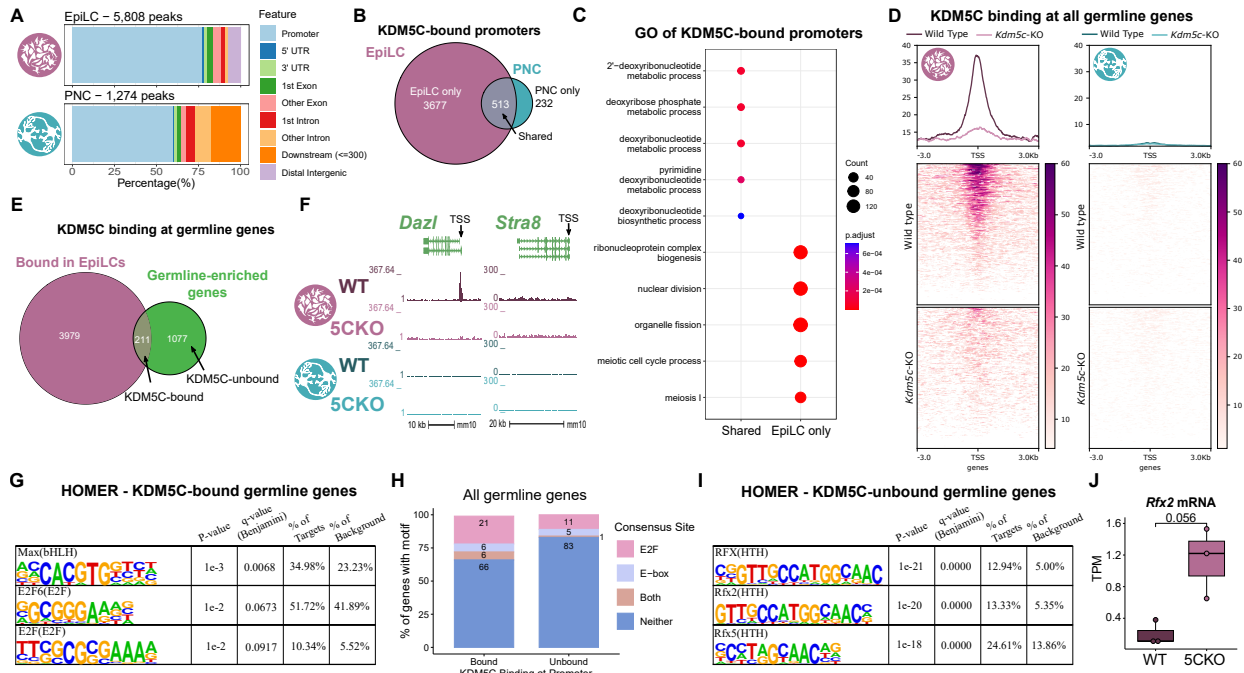


**Figure 5: KDM5C binds to a subset of germline gene promoters during early embryogenesis.** **A.** ChIPseeker localization of KDM5C peaks at different genomic regions in EpiLCs (top) and hippocampal and cortex primary neuron cultures (PNCs, bottom). **B.** Overlap of genes with KDM5C bound to their promoters ( $TSS \pm 500$ ) in EpiLCs (purple) and PNCs (blue). **C.** Gene ontology (GO) comparison of genes with KDM5C bound to their promoter in EpiLCs and PNCs. Genes were classified as either bound in EpiLCs only (EpiLC only), unique to PNCs (PNC only, no significant ontologies) or bound in both PNCs and EpiLCs (shared). **D.** Average KDM5C binding around the transcription start site (TSS) of all germline-enriched genes in EpiLCs (left) and PNCs (right). **E.** Eulerr overlap of germline-enriched genes (green) with significant KDM5C binding at their promoter in EpiLCs (purple). **F.** Example KDM5C ChIP-seq signal around the *Dazl* TSS but not *Stra8* in EpiLCs. **G.** HOMER motif analysis of all KDM5C-bound germline gene promoters, highlighting significant enrichment of MAX, E2F6, and E2F motifs. **H.** Number of all gene promoters bound or unbound by KDM5C with instances of the E2F or E-box consensus sequence. **I.** HOMER motif analysis of all KDM5C-unbound germline gene promoters, highlighting significant enrichment of RFX family transcription factor motifs. **J.** Expression of RNA-seq DEG *Rfx2* in wild-type and *Kdm5c*-KO EpiLCs. P-value of Welch's t-test, expression in transcripts per million (TPM).

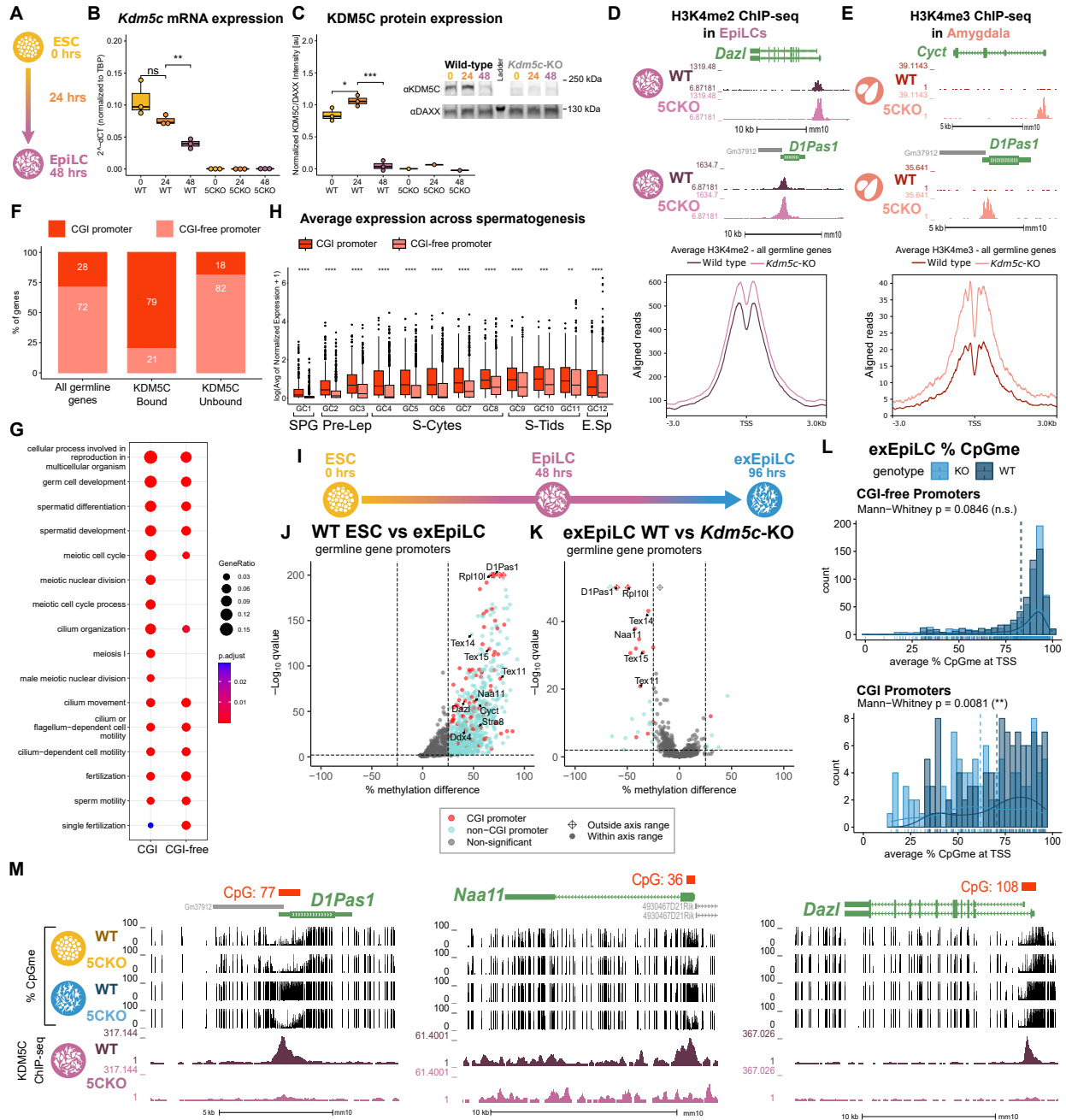


**Figure 6: KDM5C promotes long-term silencing of germline genes via DNA methylation at CpG islands.** **A.** Diagram of embryonic stem cell (ESC) to epiblast-like cell (EpiLC) differentiation and collection time points. **B.** Real time quantitative PCR (RT-qPCR) of *Kdm5c* mRNA expression in wild-type (WT) and *Kdm5c*-KO (5CKO) ESCs at 0, 24, and 48 hours of differentiation into EpiLCs. Expression calculated in comparison to TBP mRNA expression ( $2^{-\Delta\Delta CT}$ ). \*  $p < 0.05$ , \*\*  $p < 0.01$ , \*\*\*  $p < 0.001$ , Welch's t-test. **C.** KDM5C protein expression normalized to DAXX. Quantified intensity using ImageJ (artificial units - au). Right - representative lanes of Western blot for KDM5C and DAXX. \*  $p < 0.05$ , \*\*  $p < 0.01$ , \*\*\*  $p < 0.001$ , Welch's t-test. **D.** Top - Representative UCSC browser view of histone 3 lysine 4 dimethylation (H3K4me2) ChIP-seq signal at two germline genes in wild-type and *Kdm5c*-KO EpiLCs. Bottom - Average H3K4me2 signal at the TSS of all germline-enriched genes in wild-type (dark purple) and *Kdm5c*-KO (light purple) EpiLCs. **E.** Top - Representative UCSC browser view of histone 3 lysine 4 trimethylation (H3K4me3) ChIP-seq signal at two germline genes in the wild-type (WT) and *Kdm5c*-KO (5CKO) adult amygdala. Bottom - Average H3K4me3 signal at the transcription start site (TSS) of all germline-enriched genes in wild-type (dark red) and *Kdm5c*-KO (light red) amygdala. **F.** Percentage of germline genes that harbor CpG islands (CGIs) in their promoters (CGI promoter, red), based on UCSC annotation. Left - percentage of all germline-enriched genes, middle - KDM5C-bound germline genes, and right - KDM5C-unbound germline genes. (Legend continued on next page.)

**Figure 6: KDM5C promotes long-term silencing of germline genes via DNA methylation at CpG islands.** (Legend continued.) **G.** enrichPlot gene ontology analysis of germline genes with (CGI-promoter) or without (CGI-free) CGIs in their promoter. **H.** Expression of germline genes with (CGI-promoter, red) or without (CGI-free, salmon) CGIs in their promoter across stages of spermatogenesis from Green et al 2018. SPG - spermatogonia, Pre-Lep - preleptotene spermatocytes, S-Cytes - meiotic spermatocytes, S-Tids - post-meiotic haploid round spermatids, E.Sp - elongating spermatids. Wilcoxon test, \*  $p < 0.05$ , \*\*  $p < 0.01$ , \*\*\*  $p < 0.001$ , \*\*\*\*  $p < 0.0001$ . **I.** Diagram of ESC to extended EpiLC (exEpiLC) differentiation. **J.** Volcano plot of whole genome bisulfite sequencing (WGBS) comparing CpG methylation (CpGme) at germline gene promoters ( $TSS \pm 500$ ) in wild-type (WT) ESCs versus exEpiLCs. Significantly differentially methylated promoters ( $q < 0.01$ ,  $|methylated difference| > 25\%$ ) with CGIs in red, CGI-free promoters in light blue **K.** Volcano plot of WGBS of wild-type (WT) versus *Kdm5c*-KO exEpiLCs for germline gene promoters. Promoters with CGIs in red, CGI-free promoters in light blue. **L.** Histogram of average percent CpGme at the promoter of germline genes with or without CGIs. Wild-type in navy and *Kdm5c*-KO (KO) in light blue. Dashed lines are average methylation for each genotype, p-values for Mann-Whitney U test. **M.** UCSC browser view of germline genes, showing UCSC annotated CGI with number of CpGs, representative CpGme in wild-type (WT) and *Kdm5c*-KO (5CKO) ESCs and exEpiLCs, and KDM5C ChIP-seq signal in EpiLCs.